

Climate change exacerbated rainfall causing devastating flooding in Eastern South Africa

Izidine Pinto^{1,2}, Mariam Zachariah³, Piotr Wolski², Stephanie Landman⁴, Vanetia Phakula⁴, Wisani Maluleke⁴, Mary-Jane Bopape⁴, Christien Engelbrecht⁴, Christopher Jack^{1,2}, Alice McClure², Remy Bonnet⁵, Robert Vautard⁵, Sjoukje Philip⁶, Sarah Kew⁶, Dorothy Heinrich¹, Maja Vahlberg¹, Roop Singh¹, Julie Arrighi^{1,7,8}, Lisa Thalheimer^{9,11}, Maarten van Aalst^{1,7,10}, Sihan Li¹¹, Jingru Sun¹², Gabriel Vecchi^{12,13}, Wenchang Yang¹², Jordis Tradowsky¹⁴, Friederike E. L. Otto³, Romeo Dipura¹

1 Red Cross Red Crescent Climate Centre, The Hague, the Netherlands

2 Climate System Analysis Group, University of Cape Town, Cape Town, South Africa

3 Grantham Institute, Imperial College London, UK

4 South African Weather Service (SAWS), Pretoria, South Africa

5 Institut Pierre-Simon Laplace, CNRS, Sorbonne Université, Paris, France

6 Royal Netherlands Meteorological Institute (KNMI), De Bilt, The Netherlands

7 Faculty of Geo-Information Science and Earth Observation (ITC), University of Twente, Enschede, the Netherlands

8 Global Disaster Preparedness Center, American Red Cross, Washington DC, USA

9 Princeton School of Public and International Affairs, Princeton University, Princeton, NJ 08540, USA.

10 International Research Institute for Climate and Society, Columbia University, New York, USA

11 School of Geography and the Environment, University of Oxford, UK

12 Department of Geosciences, Princeton University, Princeton, NJ 08544, USA

13 High Meadows Environmental Institute, Princeton University, Princeton, NJ 08540, USA

14 Deutscher Wetterdienst (DWD), Regionales Klimabüro Potsdam, Potsdam, Germany

Main findings

- Extreme flooding occurred as a direct consequence of a 2-day heavy rainfall event at the coast of Eastern South Africa (see Fig. 1). We therefore analyse the annual maximum 2-day total rainfall in the affected area.
- The South African Weather Service and eThekweni municipality issued early warnings. There are indications, however, that the warnings had limited reach and that the people who did receive them may not have known what to do based on them.
- While the full profile of the impacts on human life and livelihoods has yet to be analysed, initial assessments show that the floods disproportionately affected marginalised communities, with particular devastation in informal settlements. Thus, the magnitude of this disaster on these groups has been exacerbated by pre-existing structural vulnerability in the region.
- The magnitude of the event is given by maximum 2-day rainfall, averaged over the homogenous area to make observations and model output comparable. The defined event

has a return time of about 20 years in today's climate in the ERA5 observational data set. An event of this magnitude would have been rarer in a 1.2°C cooler world, with a return time of about 40 years.

- At individual stations that had highest rainfall amounts, return times are much higher, e.g. 1 in 200 years at Mount Edgecombe.
- To determine the role of climate change in these observed changes we combine observations with climate models. We conclude that greenhouse gas and aerosol emissions are (at least in part) responsible for the observed increases.
- Furthermore, when taking models into account as well the changes indicate a clear increase in likelihood and intensity. We conclude that the probability of an event such as the rainfall that resulted in this disaster has approximately doubled due to human-induced climate change. The intensity of the current event has increased by 4-8%.
- Heavy rainfall events are projected to increase in frequency and magnitude in the future with additional global warming levels.

1 Introduction

On April 11-12, the eastern coast of the provinces KwaZulu-Natal (KZN) and Eastern Cape (EC) in South Africa witnessed exceptionally heavy rainfall of more than 300mm in some areas within less than 24 hours. The event was caused by a cut-off low (COL) that diverged from the mid-latitude westerly wave, and tracked across the east coast and interior of South Africa. COLs are synoptic-scale baroclinic systems that, in this region, as in other regions, can cause severe weather, heavy rainfall events and floods. COLs are a common occurrence in the month of April in this region. The impact from the April 11-12 COL was additionally exacerbated by moisture-laden, low-level maritime winds from the southern Indian Ocean (South Africa Weather Services -SAWS 2022).

The socioeconomic losses associated with this event were significant in terms of lives lost, casualties and damage to infrastructure. Over 40,000 people were impacted by the rainfall and subsequent floods- 435 deaths were reported from the affected areas, 55 injured and 54 people missing ([Government of South Africa, 2022a](#)). At least 13,500 houses were damaged or destroyed - among these, over 4,000 homes in informal settlements in eThekweni Metropolitan Municipality were destroyed, leaving 6278 people homeless and 7245 people in shelters (Ibid.). 630 schools were affected in the KZN province in the impacted areas, and 124 schools damaged, thus impacting around 270,000 students ([Government of South Africa, 2022b](#)). Critical infrastructure such as bridges and roads were also severely damaged, including two major highways ([IFRC, 2022](#)), and the mobile phone infrastructure of KwaZulu-Natal saw 400 towers impacted due to power outages and flooded fibre conduiting ([Tech Central, 2022](#)). In addition, large parts of Durban were left without electricity and water for days due to damage to water treatment and power plant stations ([IFRC, 2022](#)). The overall property damage is estimated around 17 billion rand/US\$1.57 billion ([IOL, 2022a](#)).

Fig. A shows the spatial extent and magnitude of the rainfall event on April 11 and 12, 2022. The event, as seen in the figure, and its impacts were reported to be localised over a coastal region at the east of the country.

While the most severe impacts were relatively constrained in space, the spatial scale of the synoptic system that underlies the event warrants analyses over a larger domain than that defined by maximum impact. Considering a larger area additionally enables the use of a broader range of climate models with moderate spatial resolution than those which would be defensible had a narrow, spatially-constrained definition of the event been adopted. Therefore, we define the event as the annual (July-June) maximum of 2-day accumulated rainfall, area-averaged over a domain spanning the east coast of the provinces of KwaZulu-Natal and Eastern Cape (highlighted in red in Fig. A), hereafter referred to as the East Coast-South Africa (ECSA). In that, we consider in our analyses a class of events occurring over a region characterised by a relatively homogeneous climate rather than an event of a particular rainfall intensity occurring exactly over the most impacted area. The spatial extent of the region was determined based on evaluation of homogeneity in interannual rainfall variability, rainfall seasonality, as well as geographical setting, which capture the similarity in terms of role of different rain-bearing systems such as COLs (e.g. Favre et al. 2013), tropical cyclones and tropical temperate troughs (Hart et al. 2013). The region is considered homogeneous from the perspective of evaluation of impacts of climate change at national scale (DEA, 2013, Wolski et al. 2022) (Figure S1 and S2).

Further, due to the localised nature of the impacts, we also include an alternate definition for observations where the event is the annual maximum of the local maximum 2-day average rainfall. In this study we take into account trends in heavy precipitation more generally, not limited to trends in precipitation associated with COLs only. This is intended for a realistic representation of precipitation events that are driven by various atmospheric mechanisms that can translate into floods.

In this way, we approach the attribution question from the perspective of the impact of the meteorological event of a particular magnitude, irrespective of the associated meteorological drivers.

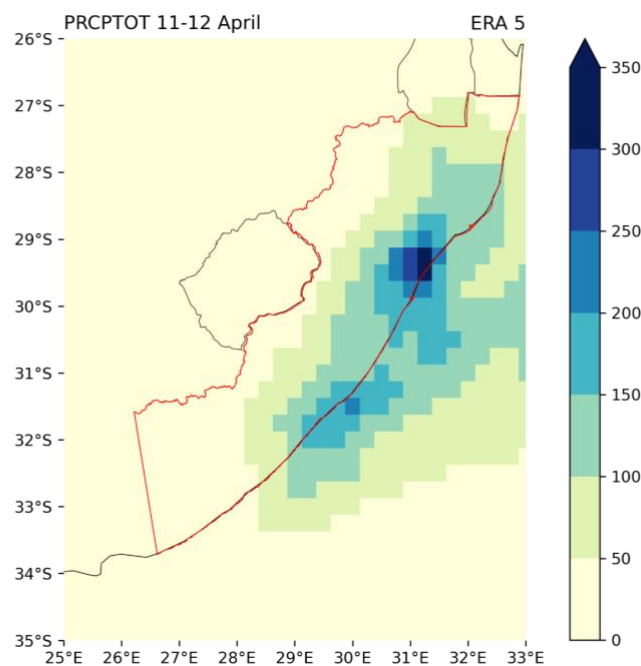


Fig. A. Average rainfall total on April 11-12, 2022 in ERA5 reanalysis data in mm/2-days. In red is the study region- East Coast-South Africa (ECSA), where the rainfall and impacts were maximum.

The major synoptic rainfall-producing weather systems over South Africa during the austral summer rainy season include tropical temperate troughs (TTT; Harrison, 1984; Hart et al., 2013), tropical weather systems such as easterly waves or lows (Tyson, 1986), ridging high pressure systems (Taljaard, 1996) and COLs (Taljaard, 1985, 1996; Muofhe et al., 2020). Of these weather systems, rainfall induced floods are typically associated with tropical lows (e.g. Triegaardt et al., 1991), landfalling tropical cyclones (e.g. Malherbe et al., 2012) and cut-off lows (e.g. Weldon and Reason, 2014). COLs can occur throughout the year, but occur most frequently during the March-May season (Singleton and Reason, 2007; Favre et al. 2013), peaking during the month of April (e.g. Engelbrecht et al., 2015). COLs are associated with widespread and intensified precipitation, contributing significantly to the annual accumulated precipitation along the south and east coasts of the country and in the transition zones between the summer and winter rainfall regions further inland (Mason and Jury, 1997; Favre et al., 2013). About 20% of COLs over the South African region are associated with heavy rainfall (Taljaard, 1985) and can therefore result in flash floods and mudslides with consequent damage to infrastructure and sometimes loss of life. For example, on 1 September 1968 more than 500 mm or rain fell over a 24-hr period in the city of Port Elizabeth due to a cut-off low (Haywood and Van den Berg, 1968). In September 1987, rainfall exceeding 900 mm over a 3-day period associated with a COL caused severe flooding affecting the coastal areas of the KwaZulu-Natal province (Singleton and Reason, 2007) with 506 lives lost (<http://www.emdat.be/>). In August 2002, a COL caused more than 300 mm or rain over a 24-hr period in East London (Singleton and Reason, 2006), situated along the Eastern Cape coast. An intense COL caused severe flooding in Port Alfred and the surrounding coastal areas from 17 to 23 October 2012 causing damages estimated at R500 million (Pyle and Jacobs, 2016). More recently, between 19-22 April 2019 a COL with its centre located over the south-western interior of South Africa produced intense precipitation, which resulted in significant damage to the infrastructure and property, and more than 80 deaths in and around the city of Durban, KwaZulu-Natal Province (Mahlangu, 2019).

Heavy rainfall is projected to increase further with warming following the Clausius-Clapeyron relationship on average, but with several regions, including Eastern Southern Africa, expected to see higher rain rates, especially on daily and shorter timescales (Seneviratne et al., 2021).

2 Data and methods

2.1 Observational data

Daily rainfall observations for 194 stations in the study domain were made available by South African Weather Service (SAWS¹). However, only around 70 stations are sufficiently gap-free and long (1950-2022) as required for assessing trends. Due to the time-sensitive nature of this study, we shortlist 5 stations that have data for the duration of the event in April 2022 for subsequent analysis. Details of these stations are provided in Table A. Therefore, we use this data in a limited manner - as an independent line of evidence for investigating precipitation trends and return period of the event at the different stations.

¹ <https://www.weathersa.co.za/home/overview>

Station	Name	Lat (°S)	Lon (°E)	Maximum 2-day accumulated rainfall, April 2022 (mm)
1.	Minnehaha Farm	30.67	30.26	205.5
2.	Emerald Dale AWS	29.94	29.96	91.4
3.	Cedara	29.54	30.27	77.6
4.	Mount Edgecombe	29.71	31.05	353.6
5.	Mapumulo Prison	29.16	31.07	184

Table A. Spatial coordinates and maximum 2-day summed rainfall totals in April, 2022 for the five SAWS stations that are shortlisted for the study.

We use the ERA5 reanalysis from the European Centre for Medium-Range Weather Forecasts (Hersbach et al., 2020) starting at year 1954, for fitting probability distributions to rainfall in the study region and thereafter for analysing the heavy rainfall event in question in the context of climate change. We note that ERA5 does not directly assimilate any rainfall observations, but rainfall is generated by atmospheric components of the IFS modelling system as a diagnostic variable. We also investigated the possibility of using satellite data products - Tropical Applications of Meteorology using SATellite data and ground-based observations (TAMSAT; Maidment et al., 2014, 2017; Tarnavsky, 2014) and Climate Hazards Group InfraRed Precipitation with Station data (CHIRPS; Funk et al. 2015), developed by analysts at the University of Reading and UC Santa Barbara, respectively. However, these datasets were excluded in the attribution study due to inconsistencies in capturing the exceptional nature of the heavy precipitation event of 11-12 April 2022.

To study the effect of climate change on rainfall distributions, we assume that the location-over-scale distribution parameter scale with the Global Mean Surface Temperature (GMST), an accepted measure of anthropogenic climate change (e.g., Luu et al., 2021; van Oldenborgh et al., 2017). We use low-pass filtered estimates of annual global mean surface temperature (GMST) from the National Aeronautics and Space Administration (NASA) Goddard Institute for Space Science (GISS) surface temperature analysis (GISTEMP, Hansen et al., 2010 and Lenssen et al. 2019).

2.2 Model and experiment descriptions

We use three different multi-model ensembles from climate modelling experiments using very different framings (Philip et al., 2020): Sea Surface temperature (SST) driven global circulation high resolution models and coupled global circulation models and regional climate models.

The first ensemble is the HighResMIP SST-forced model ensemble (Haarsma et al. 2016), the simulations for which span from 1950 to 2050. The SST and sea ice forcings for the period 1950-2014 are obtained from the 0.25° x 0.25° Hadley Centre Global Sea Ice and Sea Surface Temperature dataset that have undergone area-weighted regridding to match the climate model resolution (see Table B). For the ‘future’ time period (2015-2050), SST/sea-ice data are derived from RCP8.5 (CMIP5) data, and combined with greenhouse gas forcings from SSP5-8.5 (CMIP6) simulations (see Section 3.3 of Haarsma et al. 2016 for further details). We note here that we include only models with spatial resolution of ~60 km and less.

The second ensemble includes the AM2.5C360 (Yang et al. 2021, Chan et al. 2021) and the FLOR (Vecchi et al. 2014) climate models developed at Geophysical Fluid Dynamics Laboratory (GFDL). The AM2.5C360 is an atmospheric GCM based on that in the FLOR model (Delworth et al. 2012, Vecchi et al. 2014) with a horizontal resolution of 25 km (Chen and Lin 2011). Ten ensemble simulations of the Atmospheric Model Intercomparison Project (AMIP) experiment (1871-2020) are analysed. These simulations are initialised from ten different pre-industrial conditions but forced by the same SSTs from HadISST1 (Rayner et al. 2003) after groupwise adjustments (Chan et al. 2021), as well as the same historical radiative forcings. The FLOR model, on the other hand, is an atmosphere-ocean coupled GCM with a resolution of 50 km for land and atmosphere and 1 degree for ocean and ice. Five ensemble simulations from FLOR are analysed, which cover the period from 1860 to 2100 and include both the historical and RCP4.5 experiments driven by transient radiative forcings from CMIP5 (Taylor et al. 2012).

The third ensemble is the Coordinated Regional Climate Downscaling Experiment CORDEX-CORE (0.22° resolution, AFR-22) multi-model ensemble (Gutowski et al., 2016; Giorgi et al., 2021), comprising 10 simulations resulting from pairings of Global Climate Models (GCMs) and Regional Climate Models (RCMs) (see Table C below). These simulations are composed of historical simulations up to 2005, and extended to the year 2100 using the RCP8.5 scenario.

The 1950-2022 period for which the observed data is available is chosen for model evaluation, while the entire length of simulations up to the year 2022 is considered for the attribution analysis.

Model	Resolution	Institute
CMCC-CM2-VHR4	~25 km	Fondazione Centro Euro-Mediterraneo sui Cambiamenti Climatici
CNRM-CM6-1-HR	~50 km	Centre National de Recherches Meteorologiques
EC-Earth3P-HR	~40 km	EC-Earth-Consortium
HadGEM3-GC31-HM	~25 km	UK Met Office, Hadley Centre

HadGEM3-GC31-MM

~60 km

UK Met Office, Hadley Centre

MPI-ESM1-2-HR

~60 km

Max Planck Institute for Meteorology

Table B. List of HighResMIP models used in the study.

Regional Climate Model	Global Climate Model	Period
CanRCM4	CanESM2	1950-2100
CCLM5-0-15	HadGEM2-ES	1950-2099
CCLM5-0-15	MPI-ESM-LR	1950-2100
CCLM5-0-15	NorESM1-M	1950-2100
REMO2015	HadGEM2-ES	1970-2099
REMO2015	MPI-ESM-LR	1970-2100
REMO2015	NorESM1-M	1970-2100
RegCM4-7	HadGEM2-ES	1970-2099
RegCM4-7	MPI-ESM-LR	1970-2099
RegCM4-7	NorESM1-M	1970-2100

Table C. List of regional climate models used with their driving global climate models (see Gutowski et al., 2016 for a description of the Cordex experiment and Taylor et al. (2012) for a description of the GCMs)

2.3 Statistical methods

In this analysis we analyse the time series of July-June maximum 2-day accumulated precipitation averaged over the ECSA region where long records of observed data are available. Methods for observational and model analysis and for model evaluation and synthesis are used according to the World Weather Attribution Protocol, described in Philip et al. (2020), with supporting details found in van Oldenborgh et al. (2021), Ciavarella et al. (2021) and [here](#).

The analysis steps include: (i) trend calculation from observations; (ii) model validation; (iii) multi-method multi-model attribution and (iv) synthesis of the attribution statement. We calculate the return periods, Probability Ratio (PR; the factor-change in the event's probability) and change in intensity of the event under study in order to compare the climate of now and the climate of the past, defined respectively by the GMST values of 2022 and the pre-industrial past (1850-1900, based on the Global Warming Index <https://www.globalwarmingindex.org>). To statistically model the event under study, we use a GEV distribution that scales with GMST. Available model simulations are analysed in the same way as observations, and undergo validation tests on their statistical distributions and climatological properties. Finally, results from observations and models that pass the validation tests are synthesised into a single attribution statement.

3 Observational analysis: return time and trend

3.1 Analysis of point station data

Although the attribution analysis is performed with gridded data and an event definition that spans a regional average rather than point locations, we additionally analyse the return periods and trends in station data. This captures the impacts of the local rainfall better, and indicates differences in local trends.

Figure B shows the annual 2 day maximum rainfall trend of individual weather stations within the region of interest. 70 stations with more than 80% of valid data are used in the trend calculation. Out of 70 stations analysed, 38 stations show upward trends (statistically significant at 5 stations) while the trends are downward at 32 stations (statistically significant at 3 stations). The mixed nature of trends across the stations show that localised precipitation events and other local factors play an important role in influencing precipitation trends, in addition to climate change.

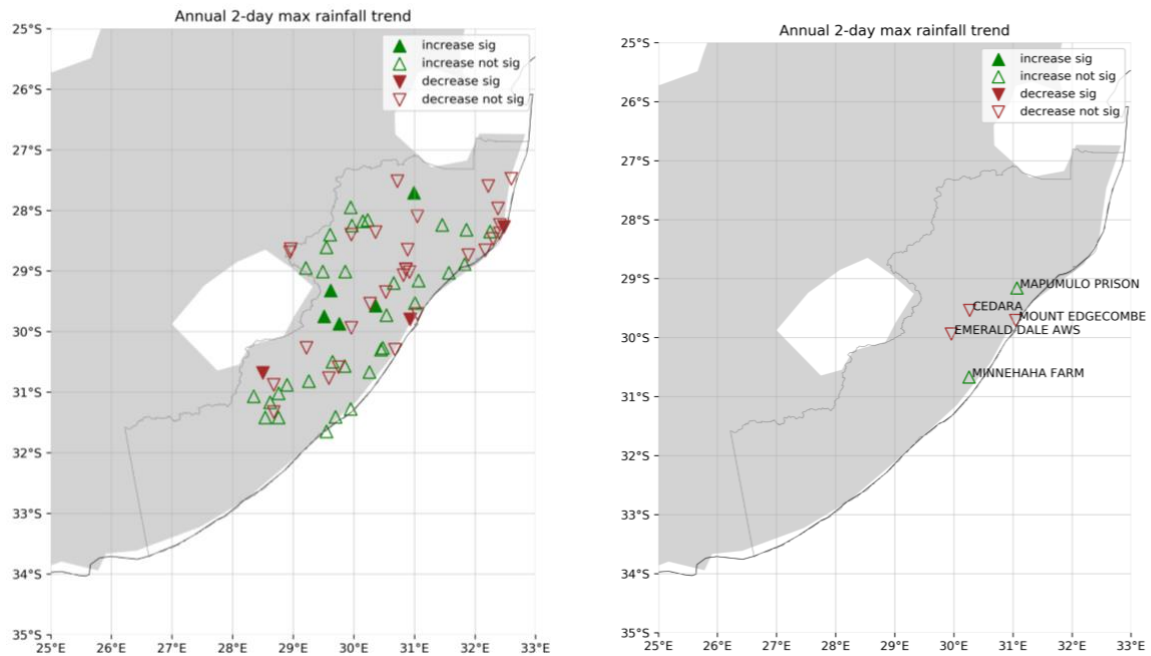


Fig. B. Annual 2 day max rainfall trend for the Weather stations within the region with 80% of data available from 1950-2022 (left) and the five stations shortlisted for this study (right). Shaded symbols indicate statistical significance at the 5% level.

We now continue with the selection of stations that have rainfall values recorded up to the event day. The annual maximum 2-day accumulated precipitation series from 1954 to 2022 for the five stations shortlisted for the study (Table A; Fig. B (right)) are shown in Fig. C. While none of these stations show a statistically significant trend, the stations in Minnehaha Farm and Mapumulo Prison tend towards an increasing trends, and the other three stations tend towards a decreasing trends.

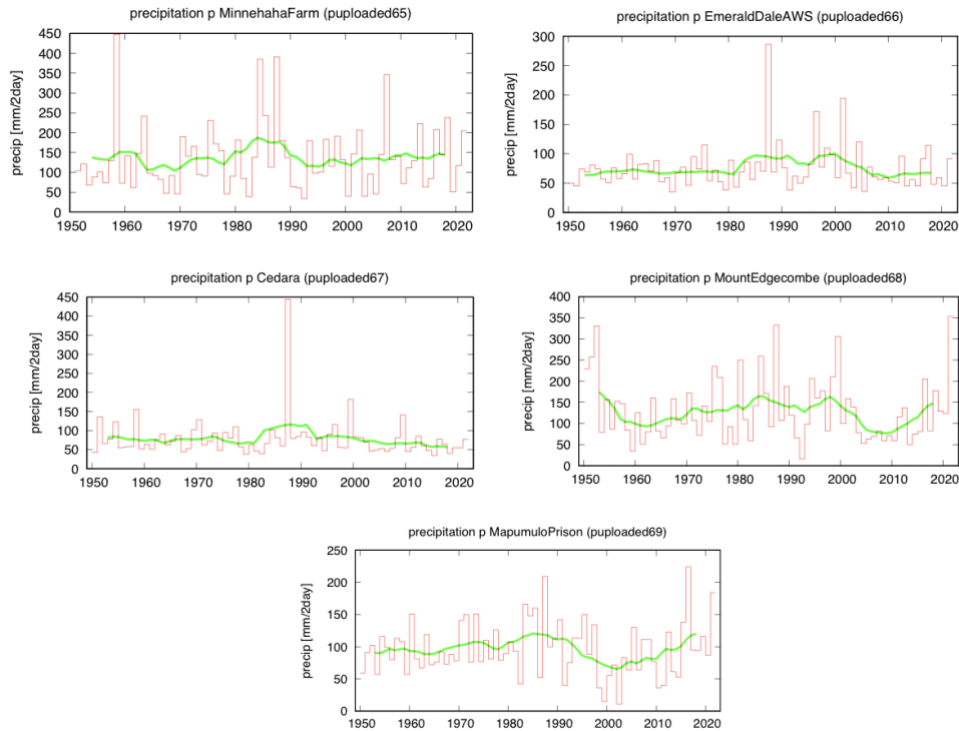


Fig. C. Time series of annual (July-June) maxima of 2-day accumulated rainfall along with the ten-year running mean (shown by green line) for Minnehaha Farm (top left), Emerald Dale AWS (top right), Cedara (middle left), Mount Edgecombe (middle right) and Mapumulo Prison (bottom).

Fig. D shows the trend fitting methods described in Philip et al. (2020) applied to the annual maximum 2-day accumulated rainfall series, for these five stations. The behaviour of the location parameter with respect to the GMST (Fig. D (left)) is variable, increasing with GMST at two locations and decreasing at the other three stations. This is to be expected, consistent with the mixed nature in the trends that we saw for the other stations in the domain (Fig. B (left)). Further, the return period of 2022 rainfall in the current climate is found to range from 1 to 200 years for these stations (Fig. D (right)). Notwithstanding the confounding effects of local factors influencing the long-term trends, these estimates corroborate that the 2022 event was indeed unusual, at least over the two stations that reported the highest rainfall during two days in April 2022- Mount Edgecombe and Mapumulo Prison (see Table A), with return periods of 1-in-200 years and 1-in-30 years, respectively.

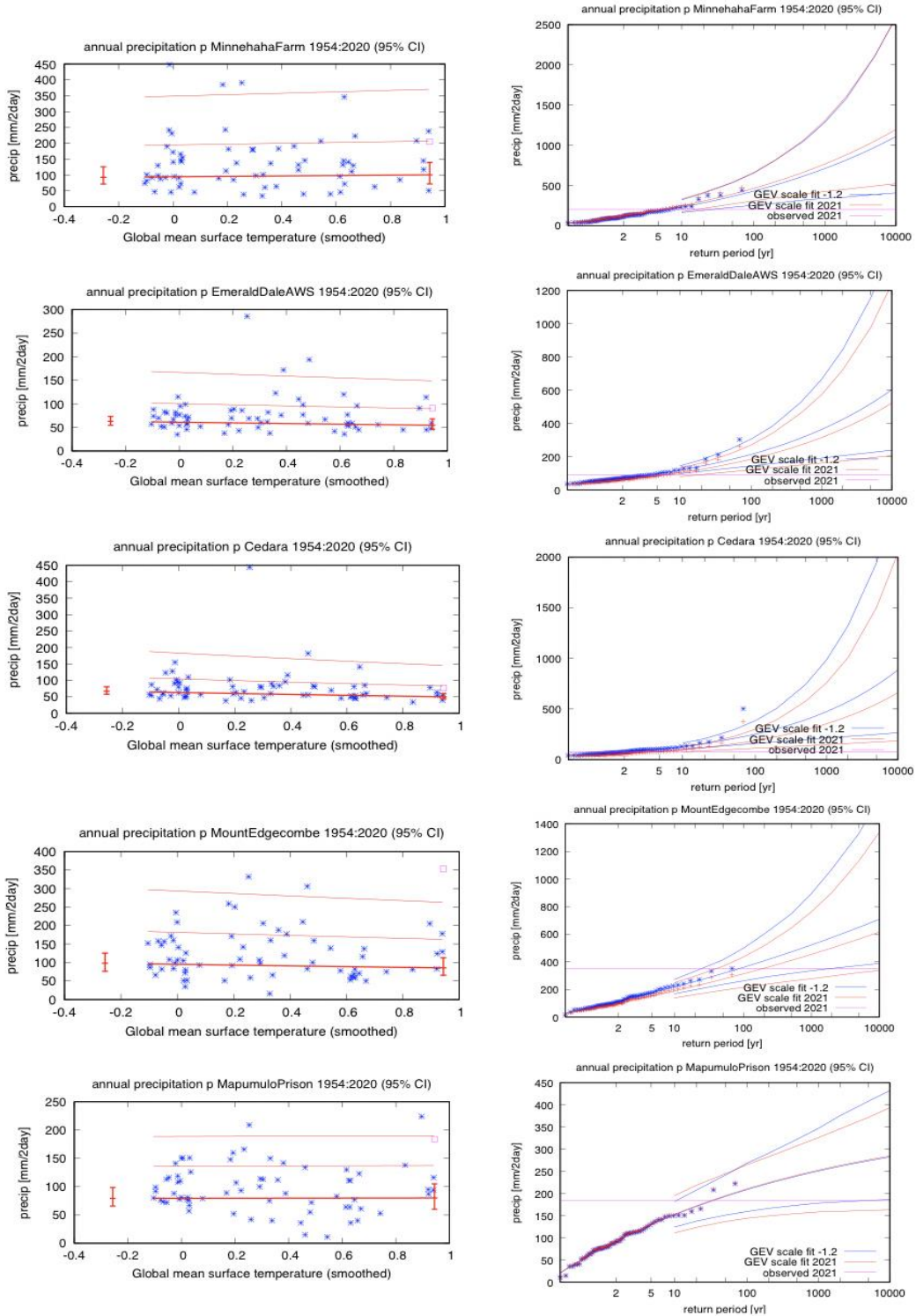


Fig. D. GEV fit with constant dispersion parameters, and location parameter scaling proportional to GMST of the index series, for the five short-listed weather stations in ECSA. No information from 2022 is included in the fit. **Left:** Observed max. annual 2-day accumulated rainfall as a function of the smoothed GMST. The thick red line denotes the time-varying location parameter. The vertical red lines show the 95% confidence interval for the location parameter, for the current, 2022 climate and the fictional, 1.2°C cooler climate. The 2022 observation is highlighted with the magenta box. **Right:** Return time plots for the climate of 2022 (red) and a climate with GMST 1.2 °C cooler (blue). The past observations are shown twice: once shifted up to the current climate and once shifted down to the climate of the late nineteenth century. The markers show the data and

the lines show the fits and uncertainty from the bootstrap. The magenta line shows the magnitude of the 2022 event analysed here.

3.2 Analysis of gridded data

Fig. E shows the time series of the area averaged ERA5 2-day averaged annual maximum precipitation and the associated GEV fit. The magnitude of the April 2022 event is 36.68 mm/day (73.4 mm over two days). The bottom left panel in Fig. E shows the response of annual maximum 2-day average precipitation to the global mean surface temperature, and the bottom right panel shows the return period curve in the current climate, the season 2021-2022, and in the past climate when the global mean temperature was 1.2 °C cooler. The return period of such an event in the current climate is 20 years (95% Confidence Interval (CI) 10 to 270 years). The trend does not (yet) emerge from natural variability, but indicates a tendency towards more and heavier precipitation events. The probability ratio is 1.8 (95% CI 0.5 to 10) and equivalently, the intensity change is 9% (95% CI -9% to 28%).

The alternative definition where the spatial maximum value is analysed rather than the average over the ECSA region gives similar results.

We note that the event was more extreme when considering only March-May (MAM) maximum values. For events happening in MAM only the return period turns out to be about 100 years (30-1000) and the positive trend does emerge from natural variability. We did not investigate this seasonal analysis further, as for the impacts it does not matter whether the event takes place in MAM or any other time in the year. Whether this analysis indicates a shift towards more extreme events later in the rainfall season also needs further investigation.

When we restrict the observational analysis to ERA5 precipitation associated with COLs only², we find strong and statistically significant upward trends in intensity of 2-day rainfall events, both for annual and MAM windows, and consequently probability ratios statistically significantly larger than 1. However, as the impacts on the ground do not depend on the origin of the precipitation we do not investigate this further here.

² We use COL identification method developed by Favre et al. 2013, adapted by Abba Omar & Abiodun (2020) applied to 1950-2022 z500 ERA5 data to identify days with COLs centres within the domain and 1 deg (~100km) buffer around it.

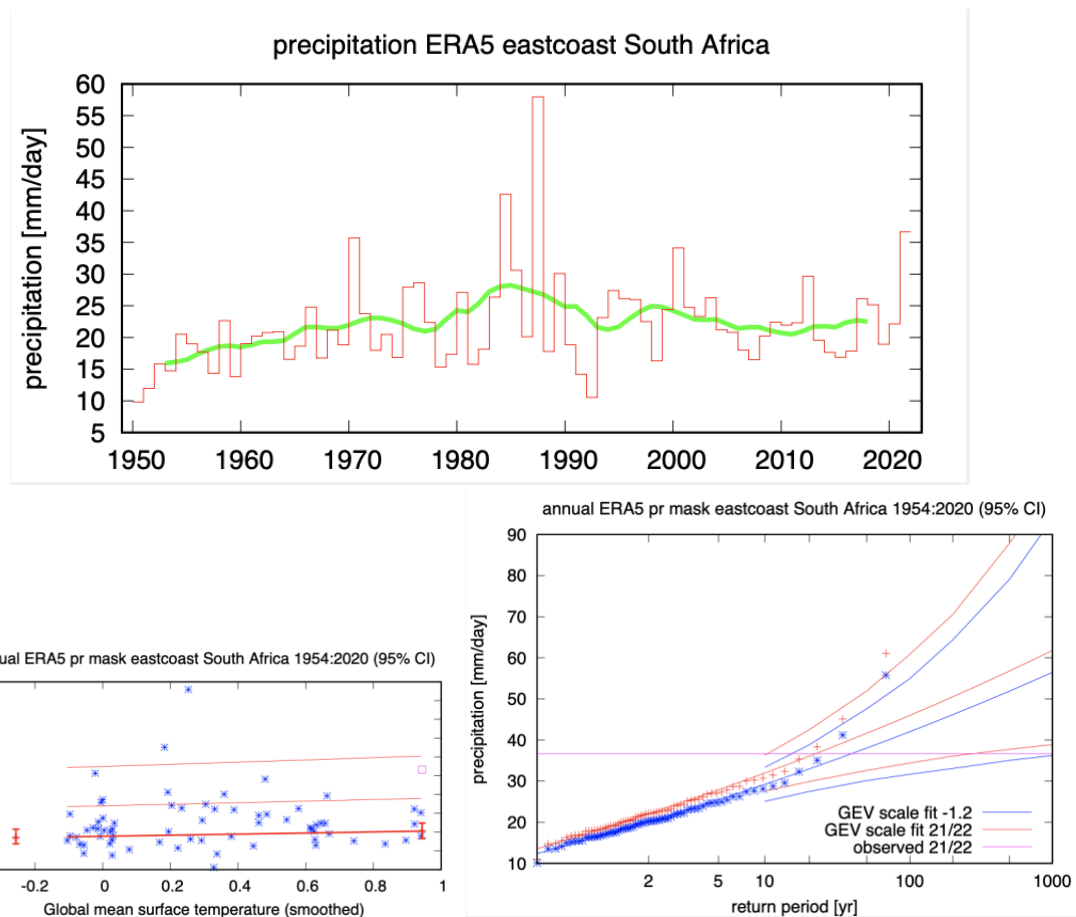


Fig. E. Top: Time series of annual (July-June) maxima of 2-day average rainfall along with the ten-year running mean (shown by green line). Bottom: GEV fit of the annual maximum 2-day average time series that scales to GMST. No information from 2022 is included in the fit. Left: Observed maximum annual 2-day average rainfall as a function of the smoothed GMST. The thick red line denotes the time-varying location parameter. The vertical red lines show the 95% confidence interval for the location parameter, for the current, 2022 climate and the 1.2°C cooler climate. The 2022 observation is highlighted with the magenta box. Right: Return time plots for the climate of 2021/22 (red) and a climate with GMST 1.2 °C cooler (blue). The past observations are shown twice: once for the current climate and once for the climate of the late nineteenth century. The markers show the data and the lines show the fits and uncertainty from the bootstrap. The magenta line shows the magnitude of the 2022 event analysed here. Source: ERA5 data.

3.3 Influence of modes of natural variability

Tropical and subtropical teleconnections, particularly the El-Niño Southern Oscillation (ENSO) is a principal driver of rainfall variability in sub-Saharan Africa (Camberlin et al., 2001). Fig. F shows the timing of wet and dry seasons associated with the negative phase of ENSO or La-Niña, for the various global regions. During the extended rainfall season in austral summer (October-March), this phase fosters positive rainfall anomalies in the parts of southern Africa, by influencing the locations of major circulations responsible for synoptic rainfall-mechanisms in these regions, primarily, the South Indian Convergence Zone (SICZ) (Hoell et al., 2015; Hart et al., 2018) and the Intertropical Convergence Zone (ITCZ; Schneider et al., 2014). The interannual variability of cut-off lows is influenced by ENSO, with above average annual frequencies of COLs occurring during La Niña years (Singleton and Reason, 2007). However, the extent to which La Nina represents a causal driver of the recent heavy rainfall over ECSA is not quantified in this study.

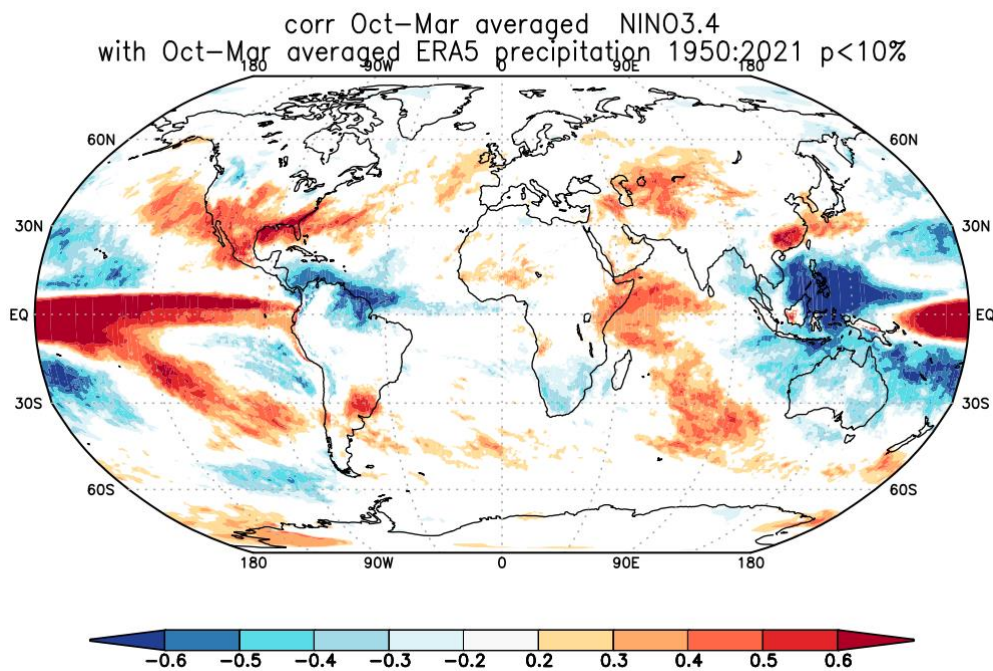


Fig. F. ENSO-rainfall relationships for October–March, using data from ERA5. Blue colours indicate that during La Niña there was, on average, more rain than normal, red colours indicate below than normal during El Niño. El Niño has the opposite effect in almost all locations. As a measure of the strength of the relationship we used the correlation coefficient with the Niño3.4 index. The square of this number gives the fraction of the variance that is explained by this aspect of El Niño.

4 Model evaluation

We use three criteria to assess the models' fitness for purpose. Firstly, we qualitatively compare the seasonal cycles in models and observations; secondly, we compare the spatial pattern of annual rainfall and thirdly, we compare the parameters of the fitted GEV in observations and models. The assessment of whether the seasonal cycles in the models follow the observed cycles. For the CORDEX simulations, for the HighResMIP models and for the GFDL climate models) is done by visually inspecting the mono-modal distributions. For the spatial patterns we compare, again visually, the annual mean rainfall in the observations with those in the models (see Fig. S3-Fig. S10).

Table D below shows the model evaluation results including both the models that passed the evaluation tests (labelled as "good", green) and models which did not meet all the validation criteria (labelled as "reasonable" (yellow)). We have applied the statistical test criteria relatively strictly, so that models where the fit parameters are only just overlapping with the observed fit parameters are only marked as "reasonable (yellow)" in the table below. Of those models considered, all that were labelled as "reasonable" were discarded from the subsequent attribution analysis, for any one of three reasons, the spatial patterns of the rainfall did not resemble those of the observations, the seasonal

cycle is wrong, or the 95% confidence intervals of the GEV parameters did not overlap with the corresponding confidence intervals in the observational data sets.

Observations	Seasonal cycle	Spatial pattern	Dispersion	Shape parameter	Event magnitude [mm/2-days]
ERAS			0.240 (0.174 ... 0.292)	0.059 (-0.16 ... 0.26)	73.35
Model					Threshold for 20-yr return period
CNRM-CM6-1-HR HighResMIP (1)	good	good	0.296 (0.238 ... 0.341)	0.15 (-0.0050 ... 0.29)	111.69
EC-Earth3P-HR HighResMIP (1)	good	good	0.211 (0.165 ... 0.246)	0.12 (-0.068 ... 0.28)	76.749
HadGEM3-GC31-HM HighResMIP (1)	good	good	0.225 (0.186 ... 0.257)	0.13 (-0.030 ... 0.28)	93.305
MPI-ESM1-2-XR HighResMIP (1)	good	good	0.267 (0.218 ... 0.303)	-0.13 (-0.31 ... 0.035)	76.098
HadGEM3-GC31-MM HighResMIP (1)	good	good	0.203 (0.165 ... 0.230)	0.18 (-0.017 ... 0.31)	100.14
CMCC-CM2-VHR4 HighResMIP (1)	good	reasonable	0.203 (0.166 ... 0.229)	-0.052 (-0.23 ... 0.095)	94.753
CanRCM4 / CanESM2 Cordex AFR-22 (1)	good	good	0.205 (0.167 ... 0.235)	-0.0040 (-0.17 ... 0.18)	78.612
CCLM5-0-15 / HadGEM2-ES Cordex AFR-22 (1)	good	good	0.231 (0.191 ... 0.262)	0.11 (-0.18 ... 0.38)	87.174
CCLM5-0-15 / MPI-ESM-LR Cordex AFR-22 (1)	good	good	0.282 (0.226 ... 0.323)	-0.0030 (-0.28 ... 0.15)	100.98
CCLM5-0-15 / NorESM1-M Cordex AFR-22 (1)	good	good	0.264 (0.207 ... 0.301)	0.043 (-0.17 ... 0.37)	95.337
REMO2015 / HadGEM2-ES Cordex AFR-22 (1)	good	good	0.220 (0.156 ... 0.260)	0.13 (-0.15 ... 0.38)	103.32
REMO2015 / MPI-ESM-LR Cordex AFR-22 (1)	good	good	0.212 (0.125 ... 0.254)	0.061 (-0.29 ... 0.61)	89.805
REMO2015 / NorESM1-M Cordex AFR-22 (1)	good	good	0.193 (0.143 ... 0.227)	-0.14 (-0.34 ... -0.0010)	86.813
RegCM4-7 / HadGEM2-ES Cordex AFR-22 (1)	reasonable	reasonable	0.246 (0.185 ... 0.289)	0.12 (-0.084 ... 0.33)	99.104
RegCM4-7 / MPI-ESM-LR Cordex AFR-22 (1)	good	good	0.284 (0.209 ... 0.338)	0.23 (0.024 ... 0.47)	92.408
RegCM4-7 / NorESM1-M Cordex AFR-22 (1)	reasonable	reasonable	0.170 (0.124 ... 0.198)	0.13 (-0.076 ... 0.39)	93.382
AM2.5C360 AMIP (10)	good	good	0.218 (0.209 ... 0.226)	0.076 (0.042 ... 0.11)	75.694
FLOR historical-rcp4.5 (5)	good	good	0.226 (0.217 ... 0.234)	0.080 (0.039 ... 0.12)	81.548

Table D. Evaluation results for the climate models considered for the attribution analysis of the annual 2-day accumulated maximum precipitation in ECSA. The table contains qualitative assessments of seasonal cycle and spatial pattern of precipitation from the models (good, reasonable) along with estimates for dispersion parameter, shape parameter and event magnitude. The corresponding estimates for ERA5 dataset is shown in blue. Based on overall suitability, the models are classified as good and reasonable, shown by green and yellow highlights, respectively.

5 Multi-method multi-model attribution

This section shows probability ratios and change in rainfall intensity (Δ) calculated from model simulations and also includes the values calculated based on observations. Table E shows these values, only for the models that are labelled “good”.

Model / Observations	Threshold for return period 20 yr	Probability ratio PR [-]	Change in intensity Δ [mm/day]
ERA5	73.75 mm/2-days	1.8(0.5 ... 9.9)	9.4 (-8.6 ... 28)
EC-Earth3P-HR HighResMIP (1)	77 mm/2-days	1.6 (0.53 ... 4.9)	9.0 (-8.2 ... 29)
HadGEM3-GC31-HM HighResMIP (1)	93 mm/2-days	1.9 (0.74 ... 12)	12 (-5.1 ... 38)
MPI-ESM1-2-XR HighResMIP (1)	76 mm/2-days	1.2 (0.19 ... 17)	1.8 (-14 ... 25)
HadGEM3-GC31-MM HighResMIP (1)	100 mm/2-days	1.0 (0.32 ... 2.1)	0.19 (-14 ... 15)
CMCC-CM2-VHR4 HighResMIP (1)	95 mm/2-days	4.6 (0.90 ... 1.1e+2)	16 (-0.68 ... 37)
CanRCM4 / CanESM2 Cordex AFR-22 (1)	79 mm/2-days	0.84 (0.25 ... 2.1)	-2.3 (-13 ... 10)
CCLM5-0-15 / HadGEM2-ES Cordex AFR-22 (1)	87 mm/2-days	0.94 (0.32 ... 6.2)	-1.1 (-18 ... 22)
CCLM5-0-15 / MPI-ESM-LR Cordex AFR-22 (1)	100 mm/2-days	2.4 (0.55 ... 6.0e+4)	14 (-6.9 ... 42)
CCLM5-0-15 / NorESM1-M Cordex AFR-22 (1)	95 mm/2-days	2.1 (0.40 ... 1.0e+3)	13 (-21 ... 63)
REMO2015 / HadGEM2-ES Cordex AFR-22 (1)	100 mm/2-days	2.6 (0.77 ... 5.0e+2)	18 (-4.4 ... 49)
REMO2015 / MPI-ESM-LR Cordex AFR-22 (1)	90 mm/2-days	1.6 (0.33 ... ∞)	7.2 (-14 ... 37)
REMO2015 / NorESM1-M Cordex AFR-22 (1)	87 mm/2-days	4.2 (0.37 ... ∞)	11 (-6.8 ... 32)
AM2.5C360 AMIP (10)	76 mm/2-days	1.8 (1.4 ... 2.4)	9.7 (3.8 ... 15)
FLOR historical-rcp4.5 (5)	82 mm/2-days	1.3 (1.1 ... 1.7)	4.7 (2.7 ... 6.8)

Table E. Precipitation threshold for the 20-yr return period, probability ratio and change in intensity for the models that passed the validation tests, for the ECSA domain

6 Hazard synthesis

For the event definition described above we evaluate the influence of anthropogenic climate change on the event by calculating the probability ratio as well as the change in intensity using observations (in this case reanalysis data ERA5) and models. Models which do not pass the validation tests described above are excluded from the analysis. We synthesise results from models that pass the validation along with the observations, to give an overarching attribution statement. Observations and models are combined into a single result in two ways if they seem to be compatible. Firstly, we neglect common model uncertainties beyond the model spread that is depicted by the model average, and compute the weighted average of models and observations: this is indicated by the magenta bar in Fig. G. As, due to common model uncertainties, model uncertainty can be larger than the model spread, secondly, we also show the more conservative estimate of an unweighted average of observations and models, indicated by the white box around the magenta bar in the synthesis figures.

Figure G shows the result of this assessment. There are no systematic discrepancies between the individual models or types of models which would be visualised by white boxes around individual model results or the observations (see e.g., <https://www.worldweatherattribution.org/wp-content/uploads/NW-US-extreme-heat-2021-scientific-report-WWA.pdf>). We therefore can use the weighted mean to indicate the main result of this study, which is for the synthesis change in probability $PR = 1.5$ (1.3 - 2.1). This corresponds to a change in intensity of 5.5 % (3.7% - 7.3%). While in the very noisy observed data the trend is not significant from a purely statistical point of view, the change in probability becomes significant (the lower bound is above 1) and the change in intensity is positive when taking the climate models into account. The increase in intensity is of the order expected from the Clausius-Clapeyron relationship and probability ratios indicate very roughly a doubling in frequency of events of this magnitude. We therefore conclude that human-caused climate change increased the probability of an event like the one observed in ECSA by approximately a factor of two and the heavy rain as observed in 2022 is a harbinger of what is to come in a warming planet.

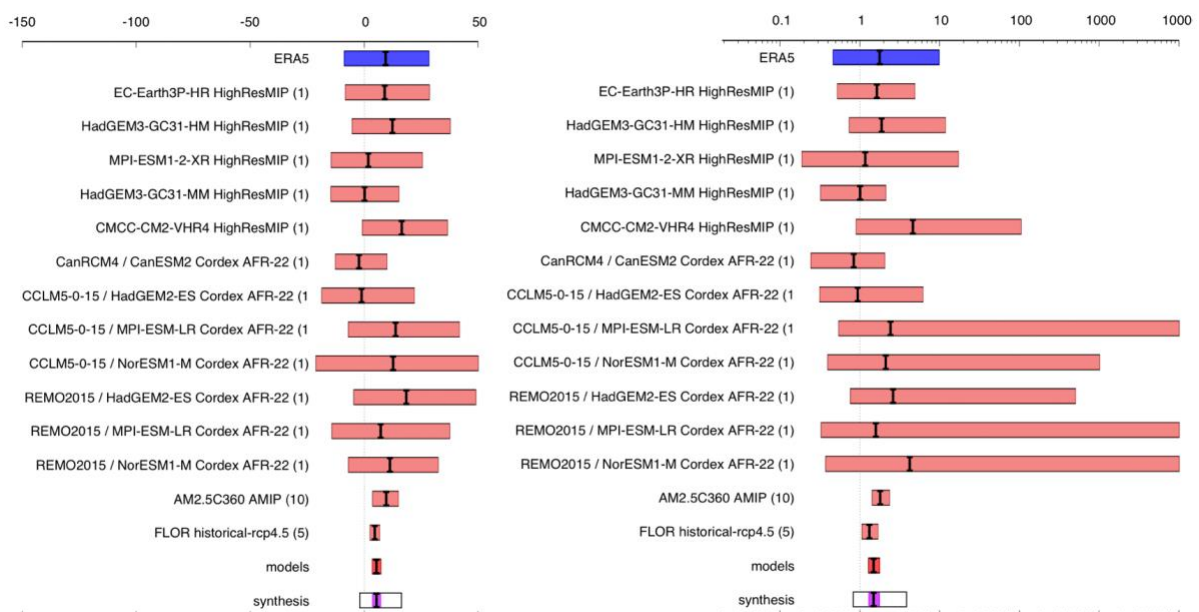


Fig. G. Synthesis of intensity change (left) and probability ratios (right), when comparing the 20-year heavy

rainfall event with a 1.2C cooler climate.

7 Vulnerability and exposure

This study estimated the return time of two-day rainfall event over a region of South Africa (Figure A) to be 20 years, while locally the return period is higher. Thus, from a meteorological perspective such an event was not unprecedented and additional factors such as the vulnerability and exposure of people, infrastructures and human systems played a role in making this meteorological event so impactful and worth studying. In this section we outline the factors that may have contributed to the impacts – as well as those that may have prevented it from becoming even worse – and summarise their implications for future floods in eThekweni municipality.

Kwazulu-Natal (KZN) is the second most populous province in South Africa with about 11.5 million people, roughly 3.5 million of whom live in the largely urban eThekweni municipality (2011 census, 2020 household survey). Between 2001 and 2011, KZN experienced an average population growth rate of 1.08% per year (2011 census). The event had disproportionate impacts on poorer and more marginalised communities, including migrants. Prior research has shown that low-income families are more likely to move in response to climatic events with Durban being one of the top 5 destination areas of internal migrants (Mastrorillo et al., 2016). Research has also shown that elderly people, children, women, people with disabilities and those disproportionately affected by structural inequality are more likely to die or be injured during floods. Whilst the full profile of the human damage of these floods has yet to be assessed, anecdotal evidence points to a similar pattern here.

7.1 Early Warning Early Action

In line with the latest guidance from the World Meteorological Organisation (WMO), the South African Weather Service (SAWS) has developed an Impact-Based Severe Weather Warning System (SWWS) for the general public. (Impact Based Severe Weather Warning System, 27/04/2022). The Impact-Based SWWS is intended to make warnings easier to understand, in order for action to be taken to mitigate adverse impacts. It involves a collaboration between SAWS and local disaster managers to determine the level of impact (minimal, minor, significant, or severe). Numerical weather prediction models and local knowledge of antecedent conditions (any previous rainfall), are used to determine the likelihood of that impact occurring (Impact Based Severe Weather Warning System, 27/04/2022).

7.1.1 Timeline of Forecast from the South African weather service (KwaZulu Natal – Durban).

- 7 April 2022, the South African Weather Service posted a media release indicating an imminent weather systems that would affect most parts of South Africa including KZN. Rainy (leading to flooding) and cold conditions were anticipated. The media release was valid from the 8th to the 11th of April 2022.

- 9 April 2022, an impact-based warning for disruptive rainfall (leading to flooding) was issued to disaster management; it was also posted on the disaster management WhatsApp group. The warning was valid for the 10th Of April 2022 (Sunday).
- 10th of April 2022, the impact-based warning was issued for disruptive rainfall (leading to flooding) in the morning valid from 10th (Sunday) to 11th (Monday) April 2022. On Sunday it was already raining across the province as SAWS continued to monitor weather developments.
- 11 April 2022 (Monday), the South African Weather Service continued to send warnings, and the weather service upgraded the warning levels twice to indicate that the situation is getting worse and the impact levels due to disruptive rainfall will be significant and severe.

The messages in these warnings indicated:

- Flooding of roads, settlements, and bridges are possible.
 - Danger to life (both human and livestock because of fast flowing streams and deep waters).
 - Possible damage to infrastructures and properties.
 - Flooding of major roads and closure, which may lead to major roads disruptions of traffic flow.
 - Difficult driving conditions on dirt roads, and possible soil erosion, rock falls and mudslides
 - Vehicle accidents are possible due to slippery roads.
- 11 April 2022, The Provincial disaster management center activated the joint operations committee, and SAWS was invited to give the weather updates to different stakeholders.

The rainfall on 11 April was equal to 75 percent of South Africa's average annual precipitation and roughly half of Durban's (BBC, 2022; Unravel Malta, 2022). While the SAWS and eThekweni municipality did forewarn the public, news reports indicate that many Durban residents have raised concerns that the eThekweni municipality did not provide them with an early warning which would have enabled preparations and evacuation, suggesting that warnings have limited reach and the people who did receive them may not know what to do based on them (The Witness, 2022).

7.2 Infrastructure, Landuse and Planning

7.2.1 Infrastructure

One of the largest impacts of the floods was to infrastructure, with roads, bridges and homes destroyed. One study found that the cost of climate change on infrastructure in South Africa could range between US\$141.0 million and US\$210.0 million average annual costs depending on the climate and adaptation scenario (Chinowsky et al., 2012). Costs would be lower, with greater investment in climate adaptation.

Following devastating 2019 floods, the City of Durban developed a 'Durban Climate Action plan 2019'. This comprehensive plan, included flood mitigation actions such as: converting 10% of hardened infrastructure to porous by 2030, public education for household level runoff reduction strategies, update rainfall and runoff projections and integrate them into flood modelling, by-law amendment to

increase flood protection in 1-100 year flood plains, incorporate updated flood lines into eThekweni Municipality's Spatial Development Framework and other spatial plans, incorporate stormwater reduction in all town planning zones, and enforce updated standards. However, this plan has only been in place for three years and is not yet fully implemented.

7.2.2 Apartheid Legacy

It is critical to recognise the legacy of apartheid spatial planning and its implications on vulnerability and exposure, and hence negative impacts of flooding and related hazards. The implementation of the Group Areas Act (GAA) by the Durban City Council in 1958 resulted in the displacement of many non-white communities into less desirable and, in some cases, more flood exposed areas. Since 1958 and despite the abolishment of the GAA and apartheid, and the establishment of non-racial democracy, strong racial and economic divides persist in South Africa. In many cases these continue to manifest in spatial patterns of housing in cities like Ethekeeni.

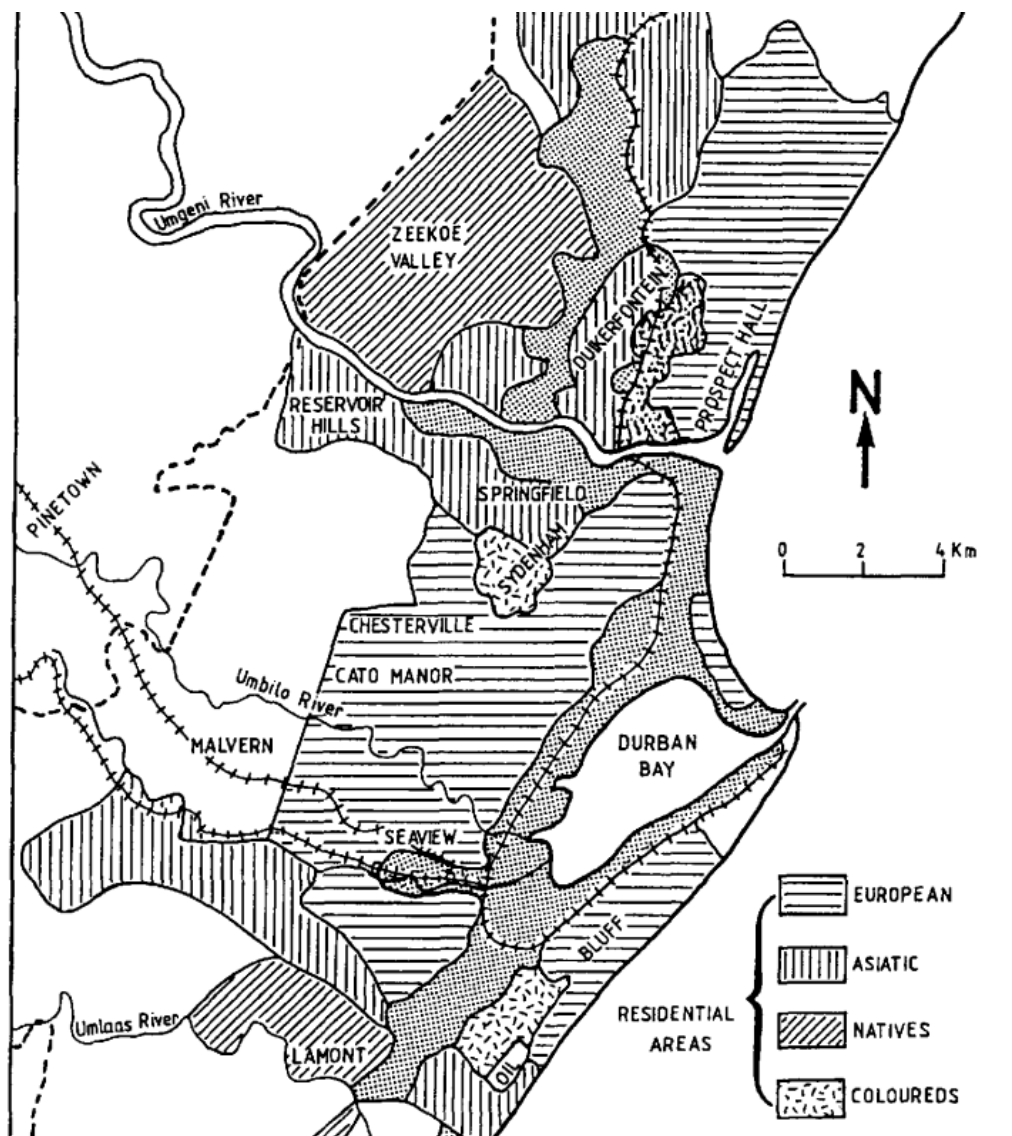


Fig. F. The Durban City Council (DCC) zoning plans, original source: Durban Housing Survey (1952), Map 11., extracted from Maharaj (1997)

7.2.3 Informal Settlements

Rapid urban growth and lack of affordable housing or land has resulted in an explosion of informal settlements in all cities in South Africa, including eThekweni ([UN-HABITAT, 2007](#)). Due to the lack of suitable land, the need to be close to employment and legacies of structural inequalities detailed in 7.2.2, informal settlements are often located on marginal sites exposed to high environmental risk and have limited social facilities and services. However, they also offer opportunities for the urban poor to claim their 'right to the city' as they are often well located in terms of job seeking opportunities, are affordable and flexible, enable self-development, and exist as a result of well-established social networks that provide a buffer to reduce risk and vulnerability. During the 2022 floods the devastation was concentrated on residents of informal settlements ([Daily Maverick, 2022](#)) and of the 13,500 homes damaged in the flooding, at least 4,000 were located in informal settlements along riverbanks ([France24, 2022](#)).

The official housing backlog of informal settlements in Durban is 238,000 households, which means that just over 800,000, or approximately 22.4% of the city's population, live in informal settlements (Misselhorn, M., 2017). Some of the severely affected areas include Umhlanga, Mpumalanga, Chatsworth, KTC Bridge City Phoenix, Umlazi, Ntuzuma, Inanda and Kwamashu.

7.2.4 Municipal vs Traditional Governance and land use management.

Spatial planning in eThekweni is complex, in part, because 38% of the municipal area is classed as rural and governed by Traditional Authorities. Customary law allows for traditional councils to allocate land to individuals for residential and subsistence purposes, resulting in a customary land right, although the state retains ownership (ITB, 2014). While land allocations occur without any municipal consultation, lease applications are reviewed by the Municipality. These customary land management practices can raise issues because they are largely unaligned with the Municipality's strategic spatial plans that provide development density, environmental and other guidelines to promote order, safety, efficient service delivery and the protection of the environmental resources within the city's boundaries. The exclusion of most residential development from planning assessment in the absence of layout plans and/or land use schemes means that the Municipality is unable to direct and manage this rapid growth to strategically plan for infrastructure services delivery. Land allocation practices ignore road reserves and servitudes leading to bulk service provision challenges, including inadequate pedestrian walkways, vehicle access and challenges of grey and storm water management. The situation is further exacerbated by the fact that the Rural Development Strategy (which should inform the scheme rollout process) was approved by Council in June 2016 but is not fully supported by traditional leaders.

7.3 Ecosystems-based Adaptation and Planning

Many interventions have been implemented in eThekweni to protect, rehabilitate and/or restore ecosystem services, with an increasing focus on the benefits of these services for reducing climate risks to communities and infrastructure. These interventions involve a range of different partnerships and have provided financial, economic, human and ecological benefits, many of which are aligned with the municipality's service delivery mandate (Mander et al., 2020).

Biodiversity protection is core principle of eThekweni's spatial planning and they have focused on protecting open/green spaces and eco-systems, including through the implementation of the Durban Metropolitan Open Space System (DMOSS). These spaces are critical for allowing flood water to drain and infiltrate into the subsurface and reducing flood extent. D'MOSS is a spatial planning tool adopted in 1989 by the former Durban City Council which has since been institutionalised and is prepared by the Environmental Planning and Climate Protection Branch (EPCPD) of eThekweni Municipality. The tool spatialises the extent of biodiversity and important ecosystems (and their services) within and around the city, and identifies areas that are suitable for urban development³.

There are 18 major river systems in eThekweni and since at least 2010, a series of riverine management projects have taken place across the municipality. This includes the Sihlanzimvelo Stream Cleaning Programme, initiated in 2012 and ongoing today, which aims to manage water flows that were undermining roads and stormwater infrastructure. It covers approximately 300km of river. (C40 2019) There is also the community-led [Aller River Pilot Project](#), beginning in 2016, focused on river restoration and invasive species removal. And the Palmiet Catchment Rehabilitation Project, focused on wetland restoration to absorb riverine flooding. Building on these experiences, in 2019, the EPCPD partnered with C40 to develop a business case to combine and scale these experiences across the city under a Transformative River Management Programme (TRMP) to reduce flood risks, among other benefits. The proposed programme would focus on removing litter, waste and invasive alien plant species from waterways to reduce blockages and create employment.

7.4 Vulnerability and Exposure Conclusion

Many factors - natural and manmade - contributed to the high death toll and damage that resulted from the 2022 Durban floods. Historical injustices that continue to affect spatial planning, governance challenges, older infrastructure, a lack of clear early warning as well as other factors that could not be fully captured in this rapid analysis, compounded upon one another to create the disaster. However, they are not unique to eThekweni as cities around the world are rapidly expanding in unplanned ways, and underlying socio-economic differences are reinforced through the built environment, increasing risk. If cities continue to develop in ways that concentrate the poorest and most marginalised people in flood prone, high risk areas, they will continue to be most affected when disaster's strike. While rainfall during this event was extreme, this type of event is not unprecedented and is likely to happen again and with even greater intensity in the future. Preventing future disasters requires rapid and inclusive adaptation that takes into account changes in both the return time of extreme weather events, and existing (and rising) vulnerability and exposure. However, there are positive signs, especially as the eThekweni municipality moves to implement existing plans around ecosystems-based adaptation, improved flood protection infrastructure and a state-of-the-art impact-based warning system.

³ <https://le.kloofconservancy.org.za/the-durban-metropolitan-open-space-system/>

Data availability

Almost all data are or will soon be available via the Climate Explorer.

For access to weather station data please contact the South Africa Weather Services (SAWS).

References

- BBC (2022). Durban floods: Is it a consequence of climate change? Available at: <https://www.bbc.com/news/61107685> [Accessed May 5, 2022].
- C40 Cities (2019). Transformative riverine management projects in Durban: background and structuring.
- Camberlin, P., Janicot, S., and Pocard, I. (2001). Seasonality and atmospheric dynamics of the teleconnection between African rainfall and tropical sea-surface temperature: Atlantic vs. ENSO. *Int. J. Climatol. A J. R. Meteorol. Soc.* 21, 973–1005.
- Chan, D., Vecchi, G. A., Yang, W., and Huybers, P. (2021). Improved simulation of 19th-and 20th-century North Atlantic hurricane frequency after correcting historical sea surface temperatures. *Sci. Adv.* 7, eabg6931.
- Chen, J.-H., and Lin, S.-J. (2011). The remarkable predictability of inter-annual variability of Atlantic hurricanes during the past decade. *Geophys. Res. Lett.* 38.
- Chinowsky, P. S., Schweikert, A. E., Strzepek, N. L., Strzepek, K. R., and Kwiatkowski, K. P. (2012). Infrastructure and climate change: Impacts and adaptations for South Africa.
- Ciavarella, A., Cotterill, D., Stott, P., Kew, S., Philip, S., van Oldenborgh, G. J., Skålevåg, A., Lorenz, P., Robin, Y., Otto, F., and others (2021). Prolonged Siberian heat of 2020 almost impossible without human influence. *Clim. Change* 166, 1–18.
- Delworth, T. L., Rosati, A., Anderson, W., Adcroft, A. J., Balaji, V., Benson, R., Dixon, K., Griffies, S. M., Lee, H.-C., Pacanowski, R. C., Vecchi, G. A., Wittenberg, A. T., Zeng, F., and Zhang, R. (2012). Simulated Climate and Climate Change in the GFDL CM2.5 High-Resolution Coupled Climate Model. *J. Clim.* 25, 2755–2781. doi:10.1175/JCLI-D-11-00316.1.
- Daily Maverick (2022). Tragedy in KZN as floods cause devastation, mostly for the poor in informal settlements. Available at: <https://www.dailymaverick.co.za/article/2022-04-12-tragedy-in-kzn-as-floods-cause-devastation-mostly-for-the-poor-in-informal-settlements/> [Accessed May 11, 2022].
- DEA (Department of Environmental Affairs) (2013). Long-Term Adaptation Scenarios Flagship Research Programme (LTAS) for South Africa. Climate Change Implications for the Water Sector in South Africa. Pretoria, South Africa.
- Engelbrecht, C. J., Landman, W. A., Engelbrecht, F. A., and Malherbe, J. (2015). A synoptic decomposition of rainfall over the Cape south coast of South Africa. *Clim. Dyn.* 44, 2589–2607. doi:10.1007/s00382-014-2230-5.
- Favre, A., Bewitson, B., Lennard, C., Cerezo-Mota, R., and Tadross, M. (2013). Cut-off Lows in the South Africa region and their contribution to precipitation. *Clim. Dyn.*, 2331–2351.
- France 24 (2022). Dozens killed in South Africa floods and mudslides following rainstorms.
- Funk, C., Peterson, P., Landsfeld, M., Pedreros, D., Verdin, J., Shukla, S., Husak, G., Rowland, J., Harrison, L., Hoell, A., and Michaelsen, J. (2015). The climate hazards infrared precipitation with stations—a new environmental record for monitoring extremes. *Sci. Data* 2, 150066. doi:10.1038/sdata.2015.66.
- Giorgi, F., Coppola, E., Teichmann, C., and Jacob, D. (2021). Editorial for the CORDEX-CORE experiment I special issue. *Clim. Dyn.* 57, 1265–1268.

- Government of South Africa (2022a). KZN flood victims to get temporary accommodation by weekend. Available at: <https://www.sanews.gov.za/south-africa/kzn-flood-victims-get-temporary-accommodation-weekend> [Accessed May 5, 2022].
- Government of South Africa (2022b). Over 600 schools impacted by KZN floods. Available at: <https://www.sanews.gov.za/south-africa/over-600-schools-impacted-kzn-floods> [Accessed May 5, 2022].
- Gutowski, W. J., Giorgi, F., Timbal, B., Frigon, A., Jacob, D., Kang, H.-S., Raghavan, K., Lee, B., Lennard, C., Nikulin, G., O'Rourke, E., Rixen, M., Solman, S., Stephenson, T., and Tangang, F. (2016). WCRP COordinated Regional Downscaling EXperiment (CORDEX): a diagnostic MIP for CMIP6. *Geosci. Model Dev.* 9, 4087–4095. doi:10.5194/gmd-9-4087-2016.
- Haarsma, R. J., Roberts, M. J., Vidale, P. L., Senior, C. A., Bellucci, A., Bao, Q., Chang, P., Corti, S., Fučkar, N. S., Guemas, V., von Hardenberg, J., Hazeleger, W., Kodama, C., Koenigk, T., Leung, L. R., Lu, J., Luo, J.-J., Mao, J., Mizielinski, M. S., Mizuta, R., Nobre, P., Satoh, M., Scoccimarro, E., Semmler, T., Small, J., and von Storch, J.-S. (2016). High Resolution Model Intercomparison Project (HighResMIP v1.0) for CMIP6. *Geosci. Model Dev.* 9, 4185–4208. doi:10.5194/gmd-9-4185-2016.
- Hansen, J., Ruedy, R., Sato, M., and Lo, K. (2010). Global surface temperature change. *Rev. Geophys.* 48.
- Harrison, M. S. J. (1984). A generalized classification of South African summer rain-bearing synoptic systems. *J. Climatol.* 4, 547–560. doi:<https://doi.org/10.1002/joc.3370040510>.
- Hart, N. C. G., Reason, C. J. C., and Fauchereau, N. (2013). Cloud bands over southern Africa: seasonality, contribution to rainfall variability and modulation by the MJO. 1199–1212. doi:10.1007/s00382-012-1589-4.
- Hart, N. C. G., Washington, R., and Reason, C. J. C. (2018). On the Likelihood of Tropical–Extratropical Cloud Bands in the South Indian Convergence Zone during ENSO Events. *J. Clim.* 31, 2797–2817. doi:10.1175/JCLI-D-17-0221.1.
- Haywood, L. O., and Van den Berg, H. (1968). Die Port Elizabeth stortreens van 1 September 1986. *S. Afr. Wea. Bureau Newsl.*, 234, 157-169.
- Hersbach, H., Bell, B., Berrisford, P., Hirahara, S., Horányi, A., Muñoz-Sabater, J., Nicolas, J., Peubey, C., Radu, R., Schepers, D., Simmons, A., Soci, C., Abdalla, S., Abellan, X., Balsamo, G., Bechtold, P., Biavati, G., Bidlot, J., Bonavita, M., Chiara, G., Dahlgren, P., Dee, D., Diamantakis, M., Dragani, R., Flemming, J., Forbes, R., Fuentes, M., Geer, A., Haimberger, L., Healy, S., Hogan, R. J., Hólm, E., Janisková, M., Keeley, S., Laloyaux, P., Lopez, P., Lupu, C., Radnoti, G., Rosnay, P., Rozum, I., Vamborg, F., Villaume, S., and Thépaut, J. (2020). The ERA5 global reanalysis. *Q. J. R. Meteorol. Soc.* 146, 1999–2049. doi:10.1002/qj.3803.
- Hoell, A., Funk, C., Magadzire, T., Zinke, J., and Husak, G. (2015). El Niño–Southern Oscillation diversity and Southern Africa teleconnections during Austral Summer. *Clim. Dyn.* 45, 1583–1599. doi:10.1007/s00382-014-2414-z.
- Hovhannissyan, S., Baum, C. F., Ogude, H. R. A., and Sarkar, A. (2018). Mixed migration, forced displacement and job outcomes in South Africa (Vol. 2) : main report (English). Washington, D.C. : World Bank Group. Available at: <http://documents.worldbank.org/curated/en/247261530129173904/main-report>.
- IFRC (2022). South Africa: Floods in KwaZulu Natal - Emergency Plan of Action (EPoA), DREF Operation MDRZA012.
- IOL (2022a). Costs related to KZN floods stands at R17 billion. Available at: <https://www.iol.co.za/mercury/news/costs-related-to-kzn-floods-stands-at-r17-billion-ca130329-5caa-40c6-8f29-346cd0f51397> [Accessed May 5, 2022].
- IOL (2022b). SA Weather Service upgrades to Orange Level 9 warning for parts of KZN, here's what it means. Available at: <https://www.iol.co.za/dailynews/news/kwazulu-natal/sa-weather-service-upgrades-to-orange-level-9-warning-for-parts-of-kzn-heres-what-it-means-dfb87d1e-0ace-47c4-be3e-bf75515abab8> [Accessed May 5, 2022].
- Lenssen, N. J. L., Schmidt, G. A., Hansen, J. E., Menne, M. J., Persin, A., Ruedy, R., and Zyss, D. (2019). Improvements in the GISTEMP Uncertainty Model. *J. Geophys. Res. Atmos.* 124, 6307–6326. doi:<https://doi.org/10.1029/2018JD029522>.
- Luu, L. N., Scussolini, P., Kew, S., Philip, S., Hariadi, M. H., Vautard, R., Van Mai, K., Van Vu, T., Truong, K. B., Otto, F., and others (2021). Attribution of typhoon-induced torrential precipitation in Central Vietnam, October 2020. *Clim. Change* 169, 1–22.
- Mahlangu, K. (2019). On the Easter weekend of 19-22 April 2019, a cut-off low (COL) weather system caused severe floods in southern parts of South Africa. Available at: <https://www.eumetsat.int/severe-floods-south-africa#:~:text=On the Easter weekend of,southern parts of South Africa.&text=The cut-off low pressure,Easter weekend in South Africa> [Accessed May 6, 2022].
- Maharaj, B. (1997). Apartheid, urban segregation, and the local state: Durban and the Group Areas Act in South Africa. *Urban Geography*, 18(2), 135-154.

- Maidment, R. I., Grimes, D., Allan, R. P., Tarnavsky, E., Stringer, M., Hewison, T., Roebeling, R., and Black, E. (2014). The 30 year TAMSAT African Rainfall Climatology And Time series (TARCAT) data set. *J. Geophys. Res. Atmos.* 119, 10,619-10,644. doi:10.1002/2014JD021927.
- Malherbe, J., Engelbrecht, F. A., Landman, W.A., and Engelbrecht, C. J. (2012). Tropical systems from the southwest Indian Ocean making landfall over the Limpopo River Basin, southern Africa: a historical perspective. *Int. J. Climatol.*, 32, 1018-1032. doi:10.1002/joc.2320
- Mason, S. J., and Jury, M. R. (1997). Climatic variability and change over southern Africa: a reflection on underlying processes. *Prog. Phys. Geogr.* 21, 23–50. doi:10.1177/030913339702100103.
- Mastrorillo, M., Licker, R., Bohra-Mishra, P., Fagiolo, G., D. Estes, L., and Oppenheimer, M. (2016). The influence of climate variability on internal migration flows in South Africa. *Glob. Environ. Chang.* 39, 155–169. doi:<https://doi.org/10.1016/j.gloenvcha.2016.04.014>.
- Misselhorn, M. (2017) Informal Settlement Upgrading eThekweni Experiences and the Incremental Services Programme (ISP) [Powerpoint Slides] Project Preparation Trust. <https://csp.treasury.gov.za/csp/DocumentsProjects/Spatial%20Targeting%20TOD%20Informal%20Settlement%20-%20Ethekeeni%20Mark%20Misselhorn.pdf>
- Muofhe, T. P., Chikoore, H., Bopape, M. J. M., Nethengwe, N. S., Ndarana, T., and Rambuwani, G. T. (2020). Forecasting intense cut-off lows in south africa using the 4.4 km unified model. *Climate* 8, 1–20. doi:10.3390/cli8110129.
- Philip, S., Kew, S., van Oldenborgh, G. J., Otto, F., Vautard, R., van der Wiel, K., King, A., Lott, F., Arrighi, J., Singh, R., and van Aalst, M. (2020). A protocol for probabilistic extreme event attribution analyses. *Adv. Stat. Climatol. Meteorol. Oceanogr.* 6, 177–203. doi:10.5194/ascmo-6-177-2020.
- Pyle, D. M., and Jacobs, T. L. (2016). The Port Alfred floods of 17-23 October 2012 : a case of disaster (mis)management? : original research. *Jamba J. Disaster Risk Stud.* 8, 1–8. doi:10.4102/jamba.v8i1.207.
- Rayner, N. A. A., Parker, D. E., Horton, E. B., Folland, C. K., Alexander, L. V, Rowell, D. P., Kent, E. C., and Kaplan, A. (2003). Global analyses of sea surface temperature, sea ice, and night marine air temperature since the late nineteenth century. *J. Geophys. Res. Atmos.* 108.
- SAWS (2022). Extreme rainfall and widespread flooding overnight: KwaZulu-Natal and parts of Eastern Cape. Available at: https://www.weathersa.co.za/Documents/Corporate/Medrel12April2022_12042022142120.pdf [Accessed April 12, 2022].
- Seneviratne, S. I., Zhang, X., Adnan, M., Badi, W., Dereczynski, C., Di Luca, A., Ghosh, S., Iskandar, I., Kossin, J., Lewis, S., Otto, F., Pinto, I., Satoh, M., Vicente-Serrano, S. M., Wehner, M., and Zhou, B. (2021). “Weather and Climate Extreme Events in a Changing Climate,” in *Climate Change 2021: The Physical Science Basis. Contribution of Working Group I to the Sixth Assessment Report of the Intergovernmental Panel on Climate Change*, eds. V. Masson-Delmotte, P. Zhai, A. Pirani, S. L. Connors, C. Péan, S. Berger, et al. (Cambridge University Press).
- Schneider, T., Bischoff, T., and Haug, G. H. (2014). Migrations and dynamics of the intertropical convergence zone. *Nature* 513, 45–53.
- Singleton, A. T., and Reason, C. J. C. (2006). Numerical simulations of a severe rainfall event over the Eastern Cape coast of South Africa: Sensitivity to sea surface temperature and topography. *Tellus*, 58A, 355-367.
- Singleton, A. T., and Reason, C. J. C. (2007). Variability in the characteristics of cut-off low pressure systems over subtropical southern Africa. *Int. J. Climatol.* 27, 295–310. doi:<https://doi.org/10.1002/joc.1399>.
- Taljaard, J. (1996). Atmospheric Circulation Systems, Synoptic Climatology and Weather Phenomena of South Africa, Part 6: Rainfall in South Africa. Technical Paper no. 32, SA Weather Bureau, Department of Environmental Affairs and Tourism, Pretoria.
- Taljaard, J. J. (1985). Cut-off lows in the South African region: South African Weather Bureau Technical Paper 14.
- Tarnavsky, E., Grimes, D., Maidment, R., Black, E., Allan, R. P., Stringer, M., Chadwick, R., and Kayitakire, F. (2014). Extension of the TAMSAT satellite-based rainfall monitoring over Africa and from 1983 to present. *J. Appl. Meteorol. Climatol.* 53, 2805–2822.
- Taylor, K. E., Stouffer, R. J., and Meehl, G. a. (2012). An overview of CMIP5 and the experiment design. *Bull. Am. Meteorol. Soc.* 93, 485–498. doi:10.1175/BAMS-D-11-00094.1.
- Tech Central (2022). Floods knock out telecoms infrastructure in KZN. Available at: <https://techcentral.co.za/floods-knock-out-telecoms-infrastructure-in-kzn/210004/> [Accessed May 5, 2022].
- The South African (2022). Regional weather forecast (temperature and uvb index) 09 April 2022. Available at: <https://www.thesouthafrican.com/news/weather/today-regional-weather-forecast-temperature-and-uvb-index-09-april-2022/> [Accessed May 5, 2022].

- The Witness (2022). KZN Floods: Durban is in a “state of disaster”, says Mayor Kaunda. Available at: <https://www.news24.com/witness/news/durban/kzn-floods-durban-is-in-a-state-of-disaster-says-mayor-kaunda-20220412> [Accessed May 5, 2022].
- Triegaard, D. O. J., van Heerden, J., and Steyn, P. C. L. (1991). Anomalous precipitation and floods during February 1988. Technical Paper no. 23, SA Weather Bureau, Department of Environmental Affairs and Tourism, Pretoria.
- Tyson, P. D. (1986). Climatic change and Variability in Southern Africa, University of the Witwatersrand. Johannesburg, Oxford University Press, Cape Town, 122-140.
- Unravel Malta (2022). Toll hits 253 in South Africa’s deadliest floods on record. Available at: <https://www.unravelmalta.com/toll-hits-253-in-south-africas-deadliest-floods-on-record-timesofmalta-com/> [Accessed May 5, 2022].
- van Oldenborgh, G. J., van der Wiel, K., Kew, S., Philip, S., Otto, F., Vautard, R., King, A., Lott, F., Arrighi, J., Singh, R., and others (2021). Pathways and pitfalls in extreme event attribution. *Clim. Change* 166, 1–27.
- van Oldenborgh, G. J., van der Wiel, K., Sebastian, A., Singh, R., Arrighi, J., Otto, F., Haustein, K., Li, S., Vecchi, G., and Cullen, H. (2017). Attribution of extreme rainfall from Hurricane Harvey, August 2017. *Environ. Res. Lett.* 12, 124009. doi:10.1088/1748-9326/aa9ef2.
- Vecchi, G. A., Delworth, T., Gudgel, R., Kapnick, S., Rosati, A., Wittenberg, A. T., Zeng, F., Anderson, W., Balaji, V., Dixon, K., Jia, L., Kim, H.-S., Krishnamurthy, L., Msadek, R., Stern, W. F., Underwood, S. D., Villarini, G., Yang, X., and Zhang, S. (2014). On the Seasonal Forecasting of Regional Tropical Cyclone Activity. *J. Clim.* 27, 7994–8016. doi:10.1175/JCLI-D-14-00158.1.
- Weldon, D., and Reason, C. J. C. Variability of rainfall characteristics over the South Coast region of South Africa. *Theor Appl Climatol.* 115, 177-185. doi:10.1007/s00704-013-0882-4.
- Wolski, P., Conradie, S., and Jack, C. (2022). Review and Recommendations on Homogeneous Climate Zones for Evaluation of Climate Change Impacts on Water Resources at the National Scale. Update of the Climate Change Status Quo Analysis for Water Resources and the Development of a Climate Change Response.
- Xiao, T., Oppenheimer, M., He, X., & Mastrorillo, M. (2022). Complex climate and network effects on internal migration in South Africa revealed by a network model. *Population and Environment*, 1-30.
- Yang, W., Hsieh, T.-L., and Vecchi, G. A. (2021). Hurricane annual cycle controlled by both seeds and genesis probability. *Proc. Natl. Acad. Sci.* 118.

Appendix

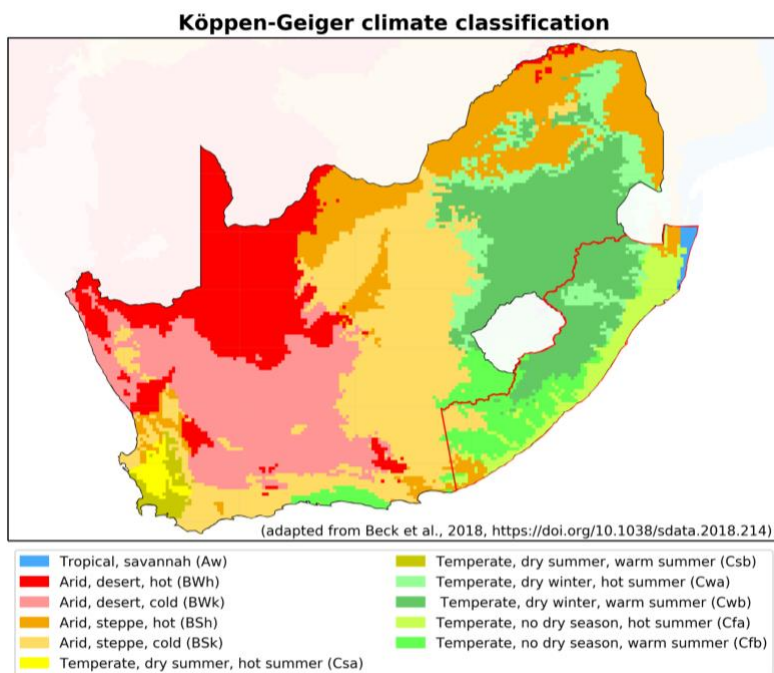


Fig. S1: Köppen-Geiger climate classifications across South Africa (source: Beck et al. 2018, <https://doi.org/10.1038/sdata.2018.214>) and the region of focus for this analysis (red lines).

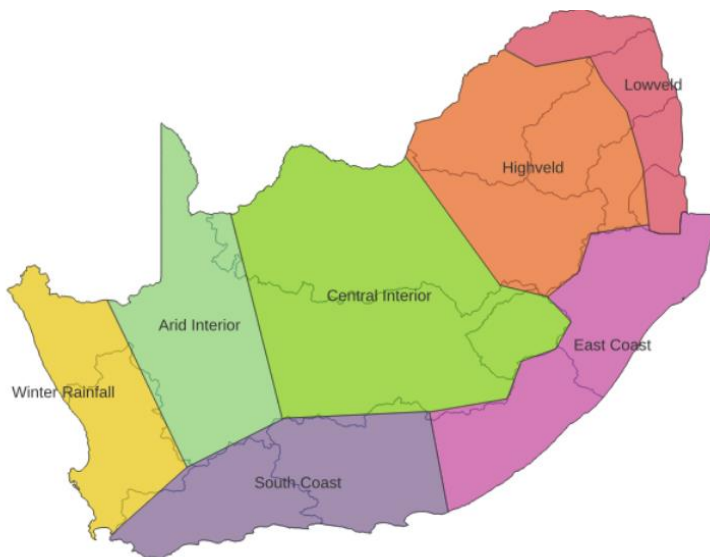


Fig. S2: Homogeneous climate zones of RSA derived by Wolski et al. 2022.

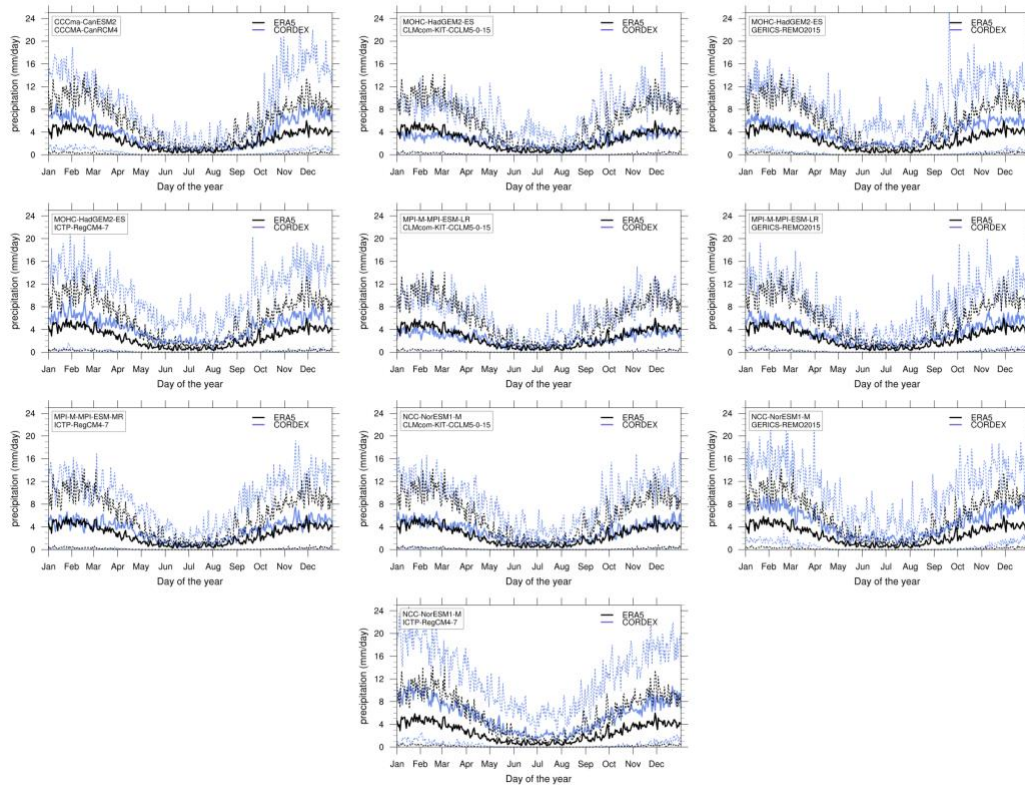


Fig. S3: Daily annual cycle of the CORDEX AFR-22 simulations (blue) calculated over the ECSA region (red region in Fig. S1) from the starting date of each Cordex simulation until 2019 and of the ERA5 observational dataset (black) calculated over the 1950-2019 period. The solid lines are the average daily annual cycle and the dash lines are the 5th and 95th quantiles.

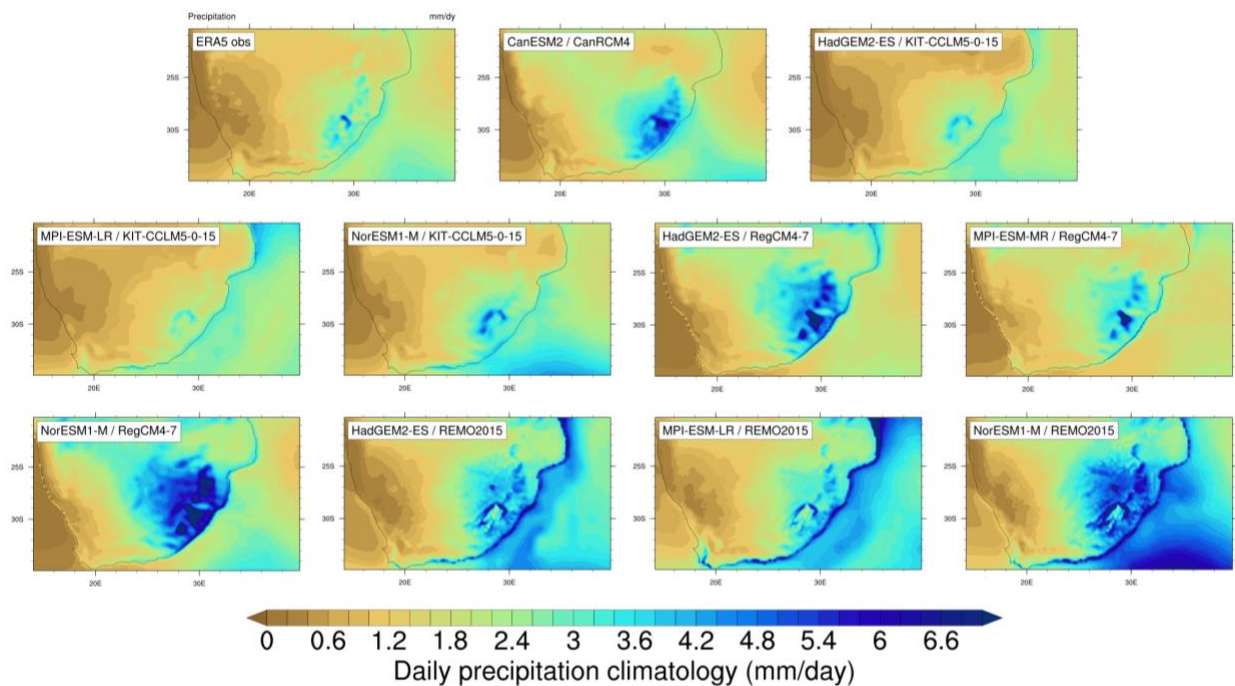


Fig. S4: Daily precipitation climatology (1970-2019) from the ERA5 observational dataset and the CORDEX AFR-22 simulations over South Africa.

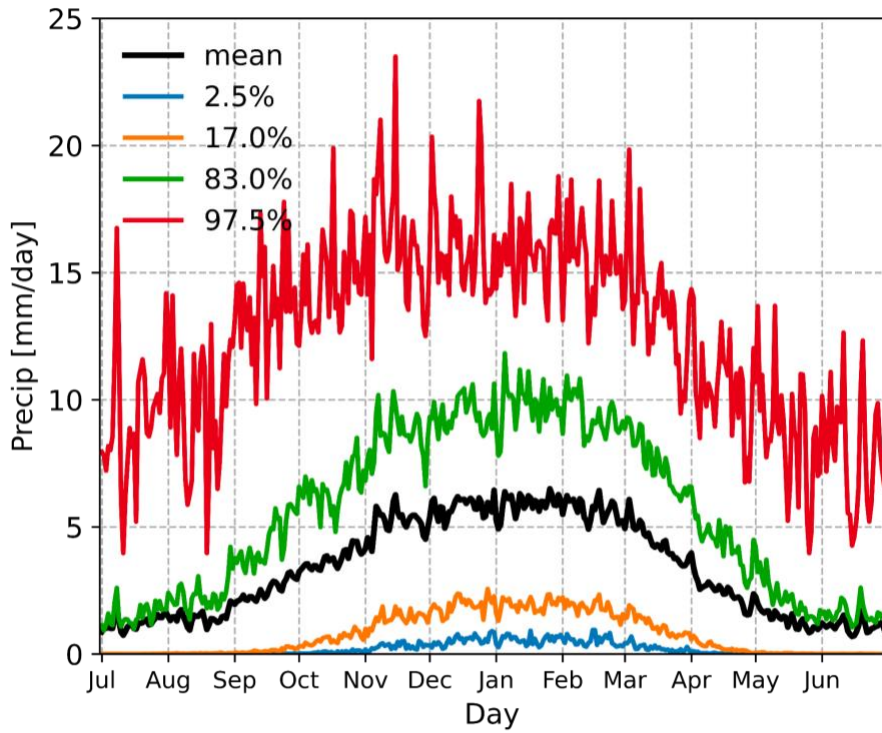


Fig. S5: Evaluation of the daily seasonal cycle (mm/day) over the ECSA region (red region in *Fig. S1*) averaged over 1990 to 2020 with the coupled FLOR model.

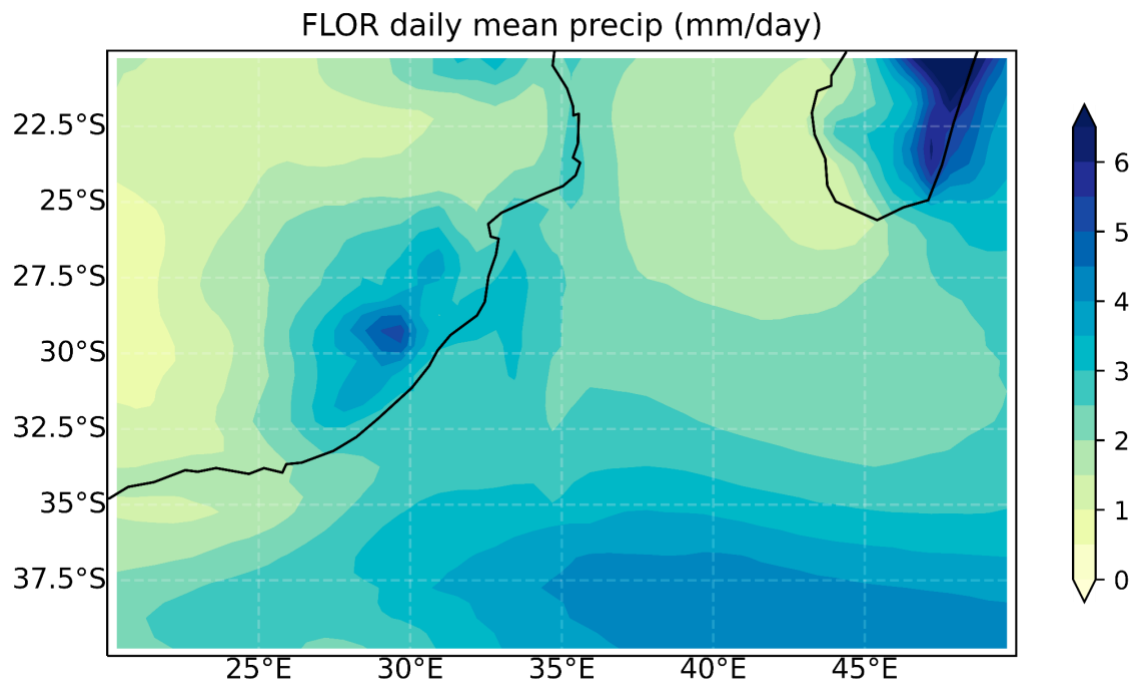


Fig. S6 Daily mean precipitation pattern for FLOR models averaged over 1990 to 2020.

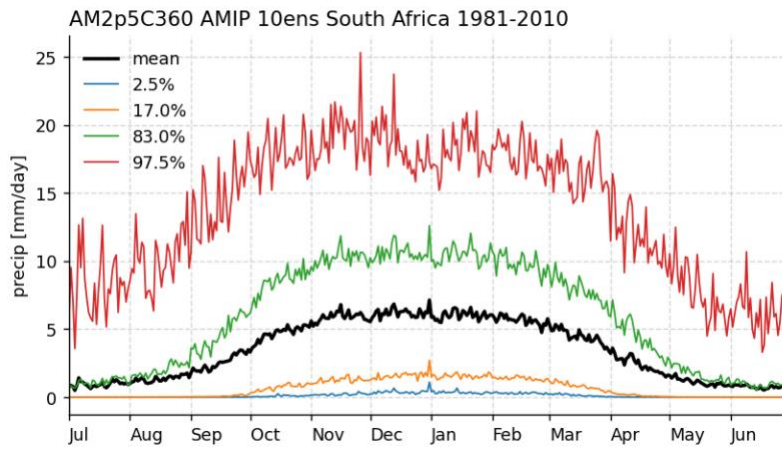


Fig. S7 Annual cycle of the daily seasonal cycle (mm/day) over the over the ECSA region (red region in *Fig. S1*) averaged over 1981 to 2010 with the AM2.5C360 model

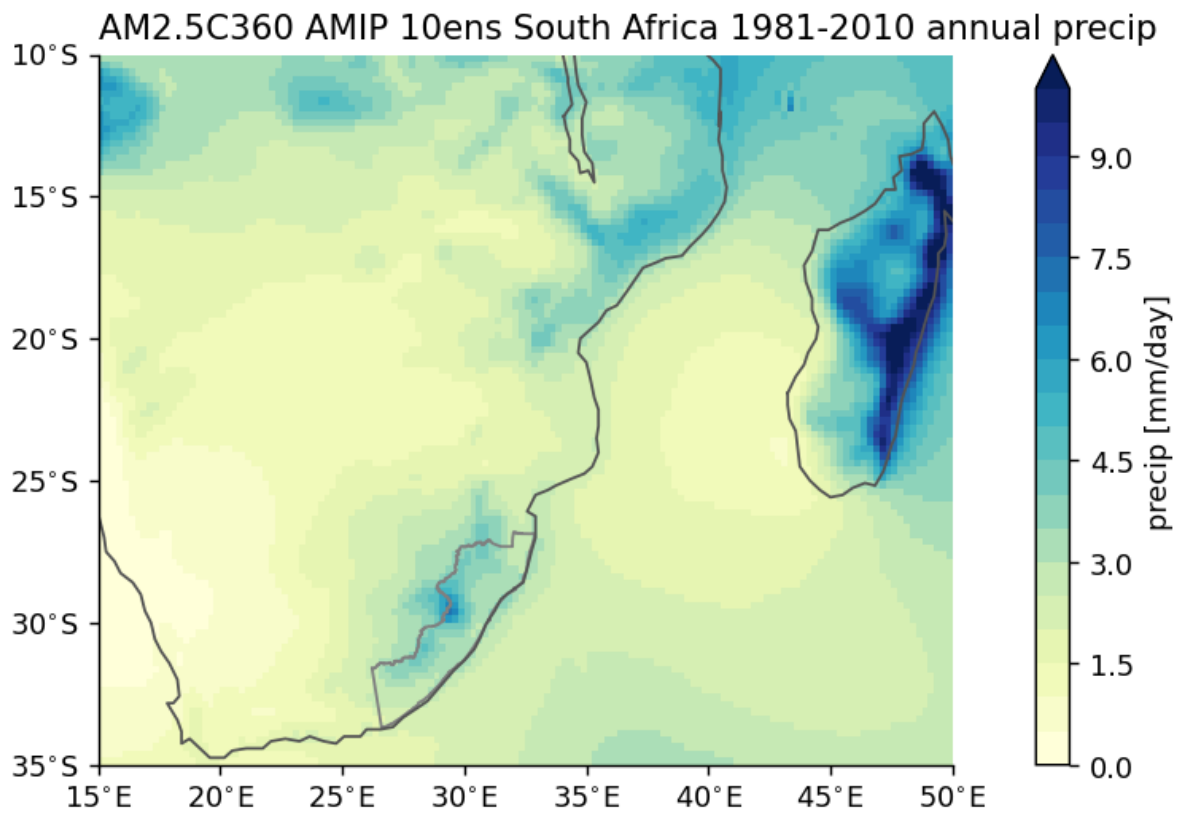


Fig. S8 Daily mean precipitation pattern for AM2.5C360 models averaged over 1981 to 2010.

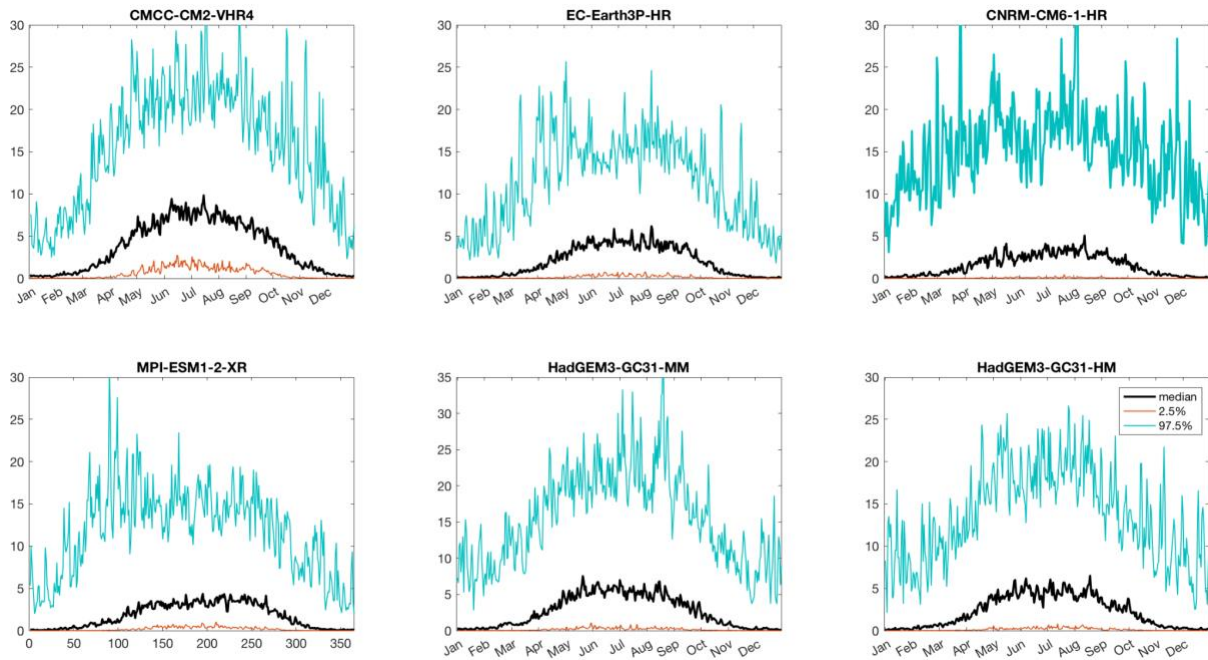


Fig. S9. Annual cycle of the daily precipitation (mm/day) over the over the ECSA region (red region in Fig. S1) averaged over 1950-2022 for HighResMIP models

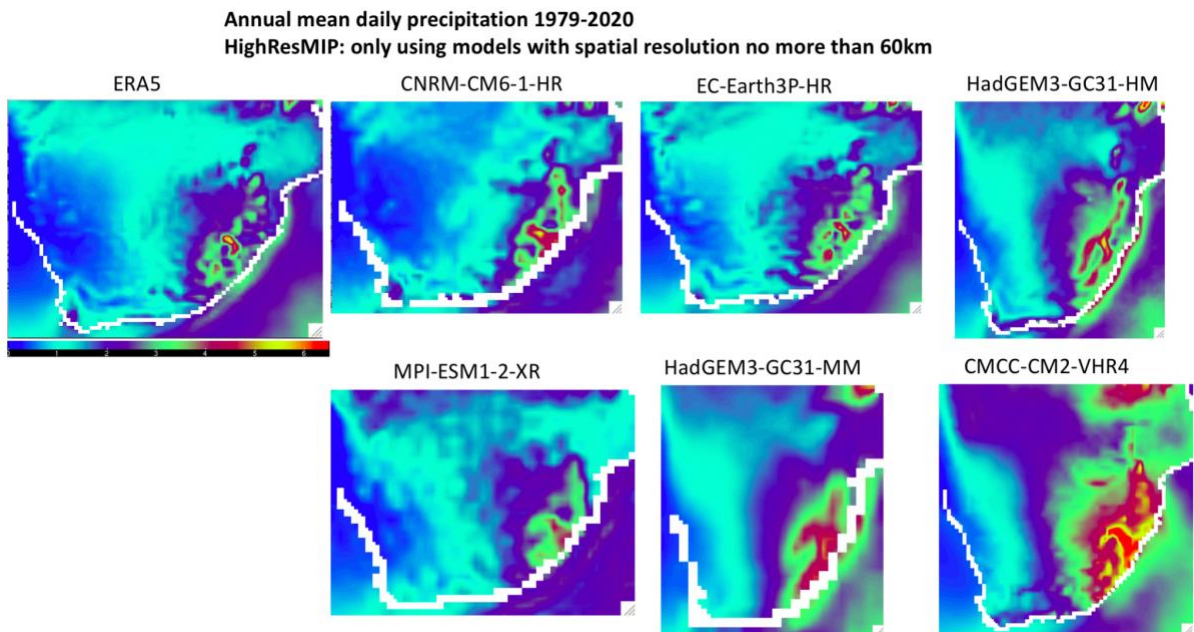


Fig. S10. Daily annual mean precipitation (mm/day) climatology (1979-2020) from the ERA5 and the HighResMIP simulations over South Africa.